Materials & Design 243 (2024) 113036

Contents lists available at ScienceDirect

Materials & Design

journal homepage: www.elsevier.com/locate/matdes

Crafting at the nanoscale: A comprehensive review of mechanical Atomic force microscopy-based lithography methods and their evolution

Lorenzo Vincenti [a,*], Paolo Pellegrino [a,b,c,*], Mariafrancesca Cascione [a,b], Valeria De Matteis [a,b], Isabella Farella [b], Fabio Quaranta [b], Rosaria Rinaldi [a,b]

[a] Department of Mathematics and Physics "Ennio De Giorgi", University of Salento, Via Monteroni, 73100 Lecce, Italy
[b] Institute for Microelectronics and Microsystems (IMM), CNR, Via Monteroni, 73100 Lecce, Italy
[c] Istituti Clinici Scientifici Maugeri IRCCS of Telese Terme Institute, 82037 Telese Terme, Italy

ARTICLE INFO

Keywords:
Mechanical-Scanning Probe-based Lithography
Atomic Force Microscopy nanolithography
Atomic Force Microscopy
Nanomachining
Nanofabrication
Nanomanipulation

ABSTRACT

In recent years, the scientific community's interest in nanoscience and nanotechnology stems from the increasing capability to manipulate matter at the nanoscale. Nanotechnology development is closely linked to fabricating and characterizing structures below 100 nm, driven by technological advancements enabling their in-depth analysis. Up to now, several top-down and bottom-up nanofabrication approaches have been developed to realize a plethora of nanostructures. Although effective, these methods have many drawbacks like high costs and limitations in feature size. In this scenario, Scanning Probe-based Lithography (SPL) emerges as a very promising alternative to conventional nanofabrication techniques, overcoming their main method limitations with versatility, flexibility, low cost, and nanoscale resolution. This review focuses on mechanical Scanning Probe-based Lithography (m-SPL), tracing its evolution from inception to recent advances. Different m-SPL methods, such as Nanoindentation, Static and Dynamic Plowing lithography, Nanomilling, and their variants are discussed in-depth, emphasizing their advantages and drawbacks, and highlighting their application. Moreover, this review explores the effects of combining m-SPL with other energy sources, such as heat and electric energy, and outlines future perspectives in the field. Overall, m-SPL stands out as a promising avenue in nanofabrication, offering sub-nanometer resolution and diverse material manipulation capabilities.

1. Introduction

The enthusiasm of the scientific community toward nanoscience and nanotechnology is rapidly increasing, as well as the capability to manipulate materials at the nanoscale is a common interest to most of the technology's fields, supported by proven applications and potential future implications. The development of nanotechnology is closely related to the capability to fabricate and characterize structures whose sizes are less than 100 nm in one or more dimensions [1,2]. Driven by the technological progress that allows in-depth analysis and manipulation of materials at the nanoscale [3,4], the nanomaterials found applications in many academic and industrial research areas. Since the invention of the integrated circuit by J. Kilby in 1959, the efforts of researchers have been focused on the development of innovative, high-throughput technological approaches to realize nanostructures and nanopatterns that are massively employed in the semiconductor industry [5] and, in particular, in electronics. In this field, the main issues concern data storage, scalability, and costs involved in the manufacturing process. However, the discovery of new, heterogeneous properties of nanomaterials, together with the progress in the nanofabrication methods, have permitted the successful employment of nanostructures in a plethora of fields, i.e. nanofluidics [6,7],

Abbreviations: AFM, Atomic Force Microscopy; CP-AFL, Constant Pulse-Atomic Force Lithography; DPL, Dynamic Plowing Lithography; EBL, Electron-Beam Lithography; ELD, electroless deposition; FIB, Focused Ion Beam Lithography; GP-AFL, Gradient Pulse-Atomic Force Lithography; LAO, Local Anodic Oxidation; m-SPL, mechanical-Scanning Probe-based Lithography; NIL, NanoImprinting Lithography; NTIL, Nanotip Indentation Lithography; P-AFL, Pulse-Atomic Force Lithography; PMMA, poly(methyl methacrylate); RIE, Reactive Ion Etching; SAM, Self-Assembled Monolayer; SATP, Standard Ambient Temperature and Pressure; SPL, Scanning Probe-based Lithography; SPM, Scanning Probe Microscopy; STM, Scanning Tunneling Microscopy; TPL, Two-Photon Lithography; TPP, two-photon polymerization; t-SPL, thermal-Scanning Probe Lithography; UNCD, ultrananocrystalline diamond.

* Corresponding authors at: Department of Mathematics and Physics "Ennio De Giorgi", University of Salento, Via Monteroni, 73100 Lecce, Italy (P. Pellegrino).
E-mail addresses: lorenzo.vincenti@unisalento.it (L. Vincenti), paolopellegrino@unisalento.it (P. Pellegrino).

https://doi.org/10.1016/j.matdes.2024.113036
Received 9 April 2024; Received in revised form 9 May 2024; Accepted 20 May 2024
Available online 22 May 2024

nanoelectronics [8–10], nano-optics [11], medicine [12], drug delivery [13], and the development of biosensors [14], antimicrobial surfaces [15,16], nano-scaffolds [17], and optical devices [18]. Indeed, the growing demand for nanostructures and nanostructured materials further supports the improvement of conventional nanofabrication techniques and the development of new strategies for the manipulation of a wide range of materials at the nanoscale [19–21]. In particular, the use of semiconductors, polymers, dielectrics, conductors, and organic materials is essential to lead the development of many fields of technology, whose perspectives could be strongly affected by nanotechnology's achievements.

To date, the major top-down approaches adopted in the nanofabrication field are photolithography [22] Electron-Beam Lithography (EBL) [23–25], Focused Ion Beam Lithography (FIB) [26], Two-Photon Lithography (TPL) [27,28], and NanoImprinting Lithography (NIL) [21]. EBL is a maskless nanolithography technique consisting of a focused electron beam that impresses an electronic resist layer. Then, the effectiveness in nanopatterning different materials is reached through the resist-developing process [24]. Although EBL is a very accurate and effective nanofabrication method, the high cost of the equipment, the slow etching rate, the necessity for further process steps, and the proximity effects make this technique unsuitable for repetitive serial production in manufacturing industrial applications [24,25]. Presently, EBL is mainly employed for manufacturing masks for optical lithography, and in academic research [29,24,25]. On the other hand, FIB is an accurate micro/nanofabrication, both top-down and bottom-up, method in which a focused ion beam is used to pattern nanostructures on several substrates directly. FIB has been used for decades to fabricate complex 3D micro-/nano- structures, easily and precisely. Indeed, it is known that FIB is not a flawless technique. However, the costs of the equipment and its maintenance are very high; extremely reliable ion beam sources and highly competent personnel are required. Differently, NIL is a molding process based on the use of a nanopatterned mask and an imprint liquid, usually a polymer, for manufacturing nanostructures on a substrate. The mask is in contact with the imprint liquid before it solidifies, thus achieving a one-to-one ratio transfer of the mask's features to the polymeric material, and finally to the substrate through an etching process. Although this technique allows a direct patterning of the nanostructures, it requires a proper mask, made using another method. In addition, the NIL method is not suitable for constructing complex 3D nanostructures [21,30]. Another effective, bottom-up, maskless nanofabrication method is the Two-Photon Polymerization (TPP). It owes its name to the non-linear absorption process involved in suitable materials and is used for manufacturing 3D free-standing micro/nanostructures beyond the diffraction limit [27,28].

A valid alternative to the nanofabrication techniques previously described is represented by Scanning Probe-based Lithography (SPL), with its wide range of different approaches, recently developed to overcome the limitation of the conventional nanofabrication methods, i.e. the cost, complexity, and efficiency for academic research and industrial applications [31–33]. The development of SPL approaches has directly followed the probe microscopy methods, which alone have brought about major advances in nanotechnology in the last decades [8,34].

Initially, the pioneering Scanning Tunneling Microscopy (STM) technique was developed in 1982, as a powerful exploitation of the quantum phenomena involving electron tunneling. Subsequently, in 1986, Binning et al. introduced Atomic Force Microscopy (AFM) [35]. AFM is a high-resolution technique which operates by leveraging the interaction between the sample's surface and a probe, influenced by either Pauli repulsion or van der Waals forces.

In AFM systems, a laser beam is focused on the cantilever apex and then reflected by its surface on a four-sectional photodiode, whose current response is recorded and used for implementing a feedback loop that drives the scanner or the probe, according to the instrument specifics [36]. This technique achieves atomic resolution, but this strongly depends on the sharpness of the tip [37].

The invention of Scanning Probe Microscopy (SPM) techniques, and the successive development of SPL, paved the way to a new paradigm of conceiving the manipulation of material at the nanoscale, that was unthinkable before. For instance, the AFM capability to interact with a material can be fully exploited by AFM-based lithography techniques, which represent the focus of this review. The instrument setting and the experimental setup, indeed, have significant advantages concerning the conventional nanofabrication method. First, the AFM tip can be employed as a nanotool to directly pattern the sample surface [38]; then, the patterned nanostructures can be immediately characterized using the same tip, avoiding further additional steps for characterization, which are required for other nanofabrication techniques. Moreover, the experimental setup itself is simple, as an AFM instrument can usually perform at the Standard Ambient Temperature and Pressure (SATP) conditions.

In the last decades, SPL approaches have been extensively exploited in both academic and industrial research fields because of their versatility, flexibility, low cost, accuracy, and nanoscale resolution [32,39,40]. To date, several types of SPL methods have been developed such as Local Anodic Oxidation (LAO) [40] or thermal [41], electric [42], dip-pen [43], and mechanical lithography [44]. In this framework, mechanical-SPL (m-SPL) is recently emerging as a very promising approach in the SPL domain, since it allows the manipulation of materials with a sub-nanometer resolution by applying a wide range of force on the sample surface, according to different operations modes [45,46]. Moreover, additional energy sources can be provided to the tip to enhance the fabrication process quality or to make it able to pattern specific materials.

This review intends to present a thorough overview and the current state of mechanical Scanning Probe-based Lithography (m-SPL) methods. It covers the evolution of these methods from their inception to the latest refined techniques, providing insights into their fabrication mechanisms. The advantages and drawbacks of the different techniques are in-depth illustrated to allow a comparison among different m-SPL approaches. Representative applications of m-SPL techniques are presented to point out their potential and critical issues. The effects of combining m-SPL with other forms of energy, for example, heat and electric energy, are discussed and future perspectives are suggested.

2. Nanoindentation and related lithography techniques

2.1. Nanoindentation

The more straightforward m-SPL technique is nanoindentation, which relies on the employment of the AFM probe to realize nanoholes or arrays of nanoholes on several materials. In nanoindentation, the tip is brought in contact with the sample surface and the probe can be further pushed toward the sample, thus causing the tip to indent the material **(**Fig. 1 **a and b)**. Typically, the curvature radius of the AFM tips at the apex ranges from a few to tens of nm, and the interested area on the sample is in the order of hundreds of nm^2 wide or less. Moreover, the tip penetrates for a depth of less than a hundred nm, and this is the reason why this technique is named nanoindentation.

Different theoretical models have been developed to describe the interaction between the material and the probe, which depends on the tip geometry and on the sample's material properties. When AFM nanoindentation is performed with a spherical-shaped tip and the indentation depth is smaller than the tip radius, the Hertz model is used to fit the data relating Young's modulus of the material to the load applied to the indenter [47], as it describes the indentation of an infinitely hard, spherical indenter on an elastic cylinder [48]. For indentation depths comparable to or exceeding the radius of curvature of the probe, the Sneddon model better describes the interaction between an infinitely hard conical indenter and an elastic cylinder [48]. Other models, based on these ones, were built to fit the presence of a pyramidal

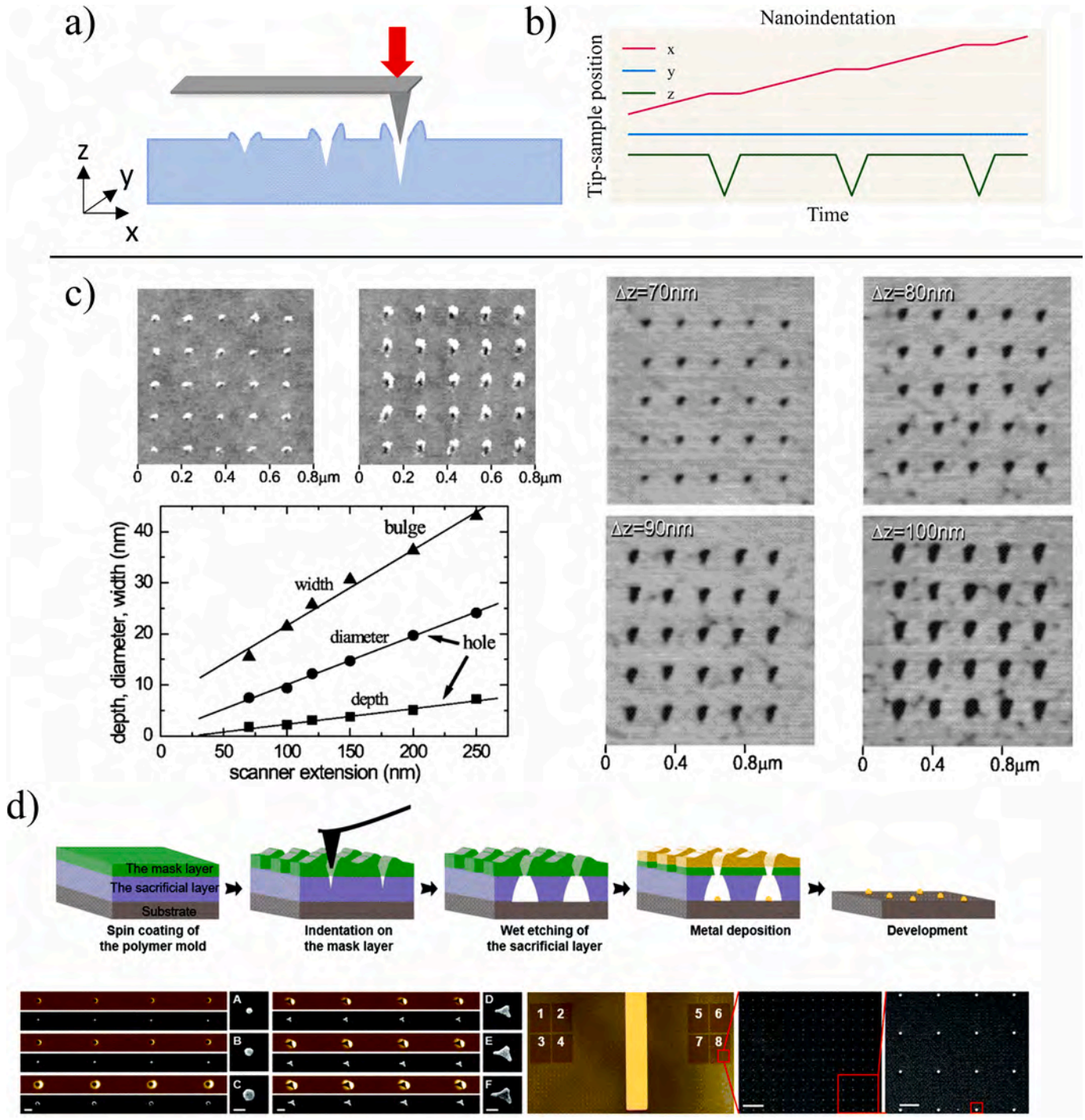

Fig. 1. AFM-based Nanoindentation technique for the nanopatterning of nanohole array. **(a)** Scheme of AFM Nanoindentation operation mode. **(b)** Graph describing the movement of the AFM probe in the *x* ,*y*, and *z* plane during the nanoindentation. **(c)** On the top panel, arrays of nanoholes generated through nanoindentation onto a 350 nm thick photoresist layer, utilizing a scanner extension, that is the variation of the scanner's height position, of 100 nm for indentation. In the bottom graph, the variation in the nanoholes depth (squares) and diameter (circles), alongside the bulge width (triangles), was plotted as a function of the scanner extension.

tip [47] or a different shape of the sample [49]. In this framework, the efforts made by G. M. Pharr, W. C. Oliver, and F. R. Brotzen resulted in a formula that can be applied when a rigid, axisymmetric punch indent an elastic half-space [47,50,51].

In 2007, N. M. Pugno developed a more sophisticated theoretical model than those previously formulated to estimate the hardness of materials through AFM-based nanoindentation [52]. The proposed model was based on the surface-to-volume ratio of the domain in which the energy flux occurs, considering the different sizes and shapes of the indenter [52]. The law derived from this approach had the previously known laws as limit cases, but it was able to fit the deviation from these models towards the nanoscale [52]. Afterward, this model was further developed, focusing on the effect related to the tip radius of curvature [53]. In order to test the model, three AFM silicon probes with different tip corner angles were nanofabricated, and nanoindentations were performed on soft material. The tip curvature radius is considered by introducing a correction factor to the hardness value obtained by a model developed for an ideal tip, which would be characterized by a

vanishing curvature radius. Then, the correction factor is applied to the experimental results to find the actual material hardness value [53]. Up to date, nanoindentation is further employed to determine the local properties of a huge range of materials, such as hardness, Young's modulus, and adhesion forces [51,54,55].

In addition to material hardness estimation, nanoindentation can be employed to plastically deform the material when an adequate force is applied. Indeed, the nanoindentation can create a nanohole on the material surface, whose geometry is determined by the tip's shape, by the normal force applied by the probe on the material's surface, and by the material's intrinsic characteristics. During the nanoindentation, the tip is subject to an increasing force due to the cantilever's bending, which is detected by the photodiode and monitored by an oscilloscope. The maximum force value and the time for a single indentation are the two parameters to be carefully set in this technique.

On the right side, nanohole grids patterned on Silicon after Reactive Ion Etching (RIE) process resulting from AFM nanoindentation on a resist, with scanner extensions of 70, 80, 90, and 100 nm, by means of Electron Beam Deposited AFM tip. Reprinted with permission from Ref. [56]. Copyright 2000 AIP Publishing LLC. **(d)** Schematic representation of the AFM indentation lithography process, followed by wet etching procedure and metal deposition, for the patterning of plasmonic nanostructures. On the bottom side images, both the nanoindentations on the mask layer and the corresponding metallic nanostructures were characterized by AFM and SEM. Scale bars correspond to 200 nm. Bright field optical microscopy images of eight nanostructures arrays (1–8) prepared using a single AFM tip and SEM images of the selected area with 4000× magnification (middle) and 10000 × magnification (right). The scale bars are 2 μm and 500 nm, respectively. Reprinted with permission from Ref. [11] Copyright © The Royal Society of Chemistry

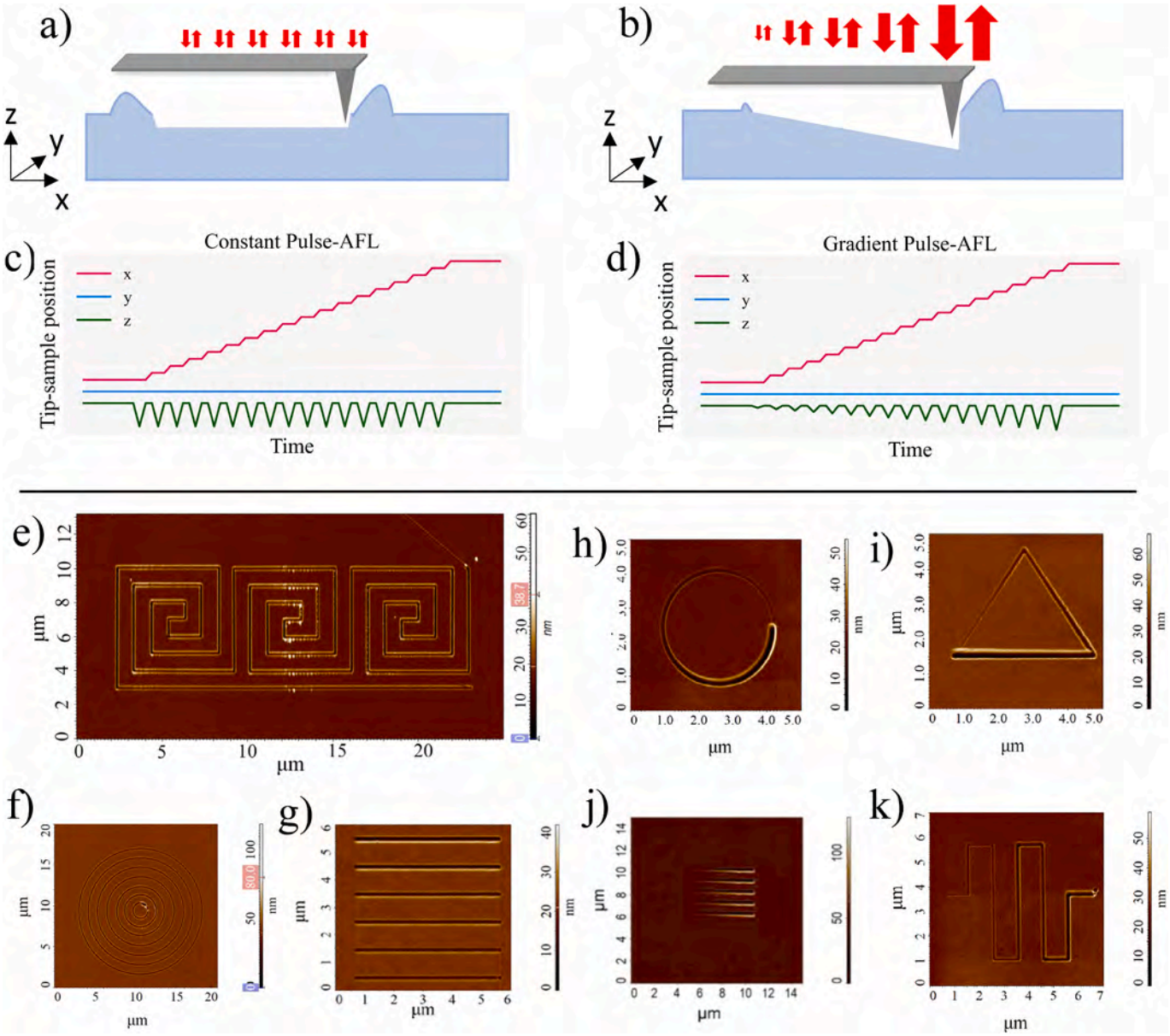

Fig. 2. Constat Pulse- and Gradient Pulse- Atomic Force Nanolithography Techniques. Sketch representation of (a) Constant Pulse and (b) Gradient Pulse – AFL; the red arrows on the AFM probes represent the force pulses used to sculpt the substrate. (c) and (d) Graphs depicting the AFM probe movement in the x ,y, and z planes during the CP- and GP- AFL, respectively. Two-dimensional, high-resolution AFM images of (e) nanolabyrinth; (f) concentric circular-shape nanostructures; (g) array of linear, parallel nanochannels; (h) Circular and (i) triangular, (j) linear and (k) serpentine-like nanostructures whit an increasing depth profile. The unconventional-shape nanostructures were fabricated on a thin PMMA layer by Constant Pulse-AFL (e-g) and Gradient Pulse-AFL (h-k). Reprinted with permission from Ref. [58,59]. Copyright 2022 MDPI.

2021.

The efficacy of nanoindentation as a nanofabrication strategy has been demonstrated and utilized by different studies, in particular on polymeric materials [56,57]. Among them B. Cappella and H. Sturm performed nanoindentations on poly(methyl methacrylate) (PMMA) at different values of the maximum normal force applied and they found a linear relation for depth up to about 160 nm [57]. K. Wiesauer and G. Springholz fabricated arrays of nanoholes on a resist layer, and then successfully transferred the pattern to the underlying Si substrate by reactive ion etching, reaching a feature's size of 7 nm [56] (Fig. 1**. c)**. More recently, J. Kim and co-workers used Nanotip Indentation Lithography (NTIL) combined with wet etching, to realize arrays of plasmonic nanodisks and nanotriangles array on a glass substrate. The shape of the nanostructures depends on the shapes of the AFM tip apex: nanodisks were realized by a conical tip while nanotriangles were patterned by means of a pyramidal-shaped probe. In detail, the glass substrates were coated with two layers of polymers: the shallower polymer film acted as a mask for the etching process while the bottom polymer layer worked as a sacrificial layer. After nanoindentation and the subsequent deposition of a gold layer, the polymer bilayers were removed (lift-off step) and the plasmonic nanostructures were successfully patterned on the glass substrate. Although this protocol may appear complex and laborious, it guarantees excellent performances in terms of precision, accuracy, and reproducibility. As an added bonus, the NTIL technique prevents degradation and damage to the tip [11] (Fig. 1**. d)**.

2.2. Pulse-atomic force Lithography

Recently, P. Pellegrino et al. proposed and optimized an alternative AFM-based lithography approach based on the nanoindentation method, termed Pulse-Atomic Force Lithography (P-AFL). The main idea is that nanoholes patterned close enough would merge into a continuous nanostructure [58,59] (Fig. 2**. a-d)**. This technique allows the patterning of nanochannels with sub-nanometric precision and high accuracy on a polymeric layer. With this method, it is possible to quickly and easily obtain 2D or 2.5D nanogrooves with the desired depth, both constant or variable, length, and slope in a single pass and without additional energy sources [58].

In detail, the P-AFL comes in two different variants: Constant Pulse-Atomic Force Lithography (CP-AFL) and Gradient Pulse-Atomic Force Lithography (GP-AFL), which enable the fabrication of nanogrooves with constant or gradient depth profiles, respectively [58]. In the latter case, the grooves change their profile smoothly and continuously. The difference between the CP-AFL and the GP-AFL technique is that in the first one the indentations are performed all with the same normal force value, while in the second one its intensity linearly increases for successive nanoindentations [58,60] (Fig. 2 **c and d)**.

P-AFL techniques were employed for patterning various complex shapes, circular, triangular, and serpentine-like on a polymer substrate [59] (Fig. 2 **e-k)**. Moreover, 2D and 2.5D nanostructures can be patterned on a resist layer and transferred to the underlying, harder material by conventional plasma etching with high fidelity and reproducibility [58].

2.3. Plowing Lithography

The term "plowing lithography", related to AFM-based lithography, refers to m-SPL techniques developed from two conventional AFM imaging modes: contact and semicontact mode. While in AFM imaging tip contact must leave the sample unmodified, in plowing lithography greater normal forces are exerted on the material's surface by the tip, and scratches or nanogrooves are obtained due to the motion of the tip relative to the substrate.

In the Static Plowing Lithography technique, the AFM probe is in contact with the sample to scratch its surface by moving forward and backward along a grid of lines with the suitable force to shape the material (Fig. 3 **a and b)**. In order to obtain well-defined nanostructures, several parameters must be carefully set, such as the interaction force, the scanning direction, the scanning rate, and the material to be patterned has to be carefully selected [61]. A. A. Tseng et al. explored the possibility to fabricate nanogrooves and nanodots by Static Plowing Lithography on a 30 nm $Ni_{80}Fe_{20}$ thin film deposited on a Si substrate by scratching the surface with a diamond-coated tip, characterized by an apex radius between 115 nm and 125 nm, and loaded with a normal force of 9 μN [62] (Fig. 3 **c)**. At first, arrays of nanogrooves of almost 15 nm in depth were patterned respectively with a pitch of 80 nm and 35 nm, that is the distance between two adjacent grooves. Then, an array of lines was scratched on the 35 nm pitch array, respecting the same pitch but in the perpendicular direction, thus obtaining a quasi-3D nanostructure consisting of an array of evenly distributed hemispheric quantum dots, which had a dot density of 2.6×10^8 per mm^2 [62–66] (Fig. 3 **c)**.

L. A. Porter et al. developed a nanofabrication process to successfully pattern gold nanoparticles and nanowires on semiconductor Ge(1 1 1). First, they spun a (20 ± 2) nm photoresist layer on a substrate of Ge (1 1 1). Then, they performed Static Plowing Lithography by using a silicon tip loaded with a normal force in the range from 3 μN to 5 μN, and a scan rate of 100 μm/s [61]. It resulted in nanogrooves that reached the underlying Ge substrate. Finally, the sample was immersed in a solution of $HAuCl_4$, letting the Au deposit on the semiconductor's exposed surface, where it shaped into nanoparticles that grew and merged to form nanowires [61]. Similarly, S. B. Ulapane et al. developed an innovative method for the deposition of metal microstructures on different substrates [67]. By using silicon glass and mica as substrates, they deposited on them a uniform thin film of $CaCO_3$ NPs, previously synthesized and diluted to a proper concentration. To remove the resist material from square areas on the substrate, the Static Plowing Lithography technique was optimized by varying the scanning rate, the applied normal force, and the number of passes. Then, a uniform film of gold was evaporated, and the remaining $CaCO_3$ NPs layer was dissolved in an aqueous solution, leaving a gold square microplatform on the substrate [67] (Fig. 3 **d)**.

In AFM Static Plowing Lithography, a very high resolution can be obtained by patterning Self Assembled Monolayers (SAMs) on flat substrates with a very sharp tip, characterized by a tip radius of the order of the nm or less. In this framework, C. M. Edwards et al. investigated the possibility to fabricate copper, silver, and gold nanostructures on silicon (Si) substrates through the nanopatterning of a SAM resist by AFM nanolithography, followed by metal deposition in the structure using electroless deposition (ELD) [68]. The substrate doping, SAM composition, and AFM scanning parameters were optimized, and the ELD solution capability to selectively deposit metals on exposed areas of the Si surfaces was demonstrated [68].

A further step towards AFM application at molecular resolution can be made by working with AFM in liquid media. The SAMs imaging is performed in contact mode under very low normal forces, to avoid damaging the monolayer. Based on Static Plowing Lithography, two different methods can be developed to pattern the SAM in liquid media, depending on the desired result: nanoshaving and nanografting [69]. In both cases, a normal force greater than the molecules' displacement threshold must be applied. However, while nanoshaving is completely analog to Static Plowing Lithography as previously described, in nanografting technique, different molecules are introduced in solution to replace the SAM molecules when they are mechanically displaced by the AFM tip [69].

Static Plowing Lithography can be used to pattern complex 2D geometrical figures in a very short time because the scan rates could be set up to about tens to hundreds of μm/s [61]. For asymmetrical probes, to maintain a constant scratching direction and not affect the quality of nanostructures with undesired effects due to the lateral force and the tip orientation, the sample must be rotated during the scratching process [70]. In addition to the aforementioned Static Plowing Lithography

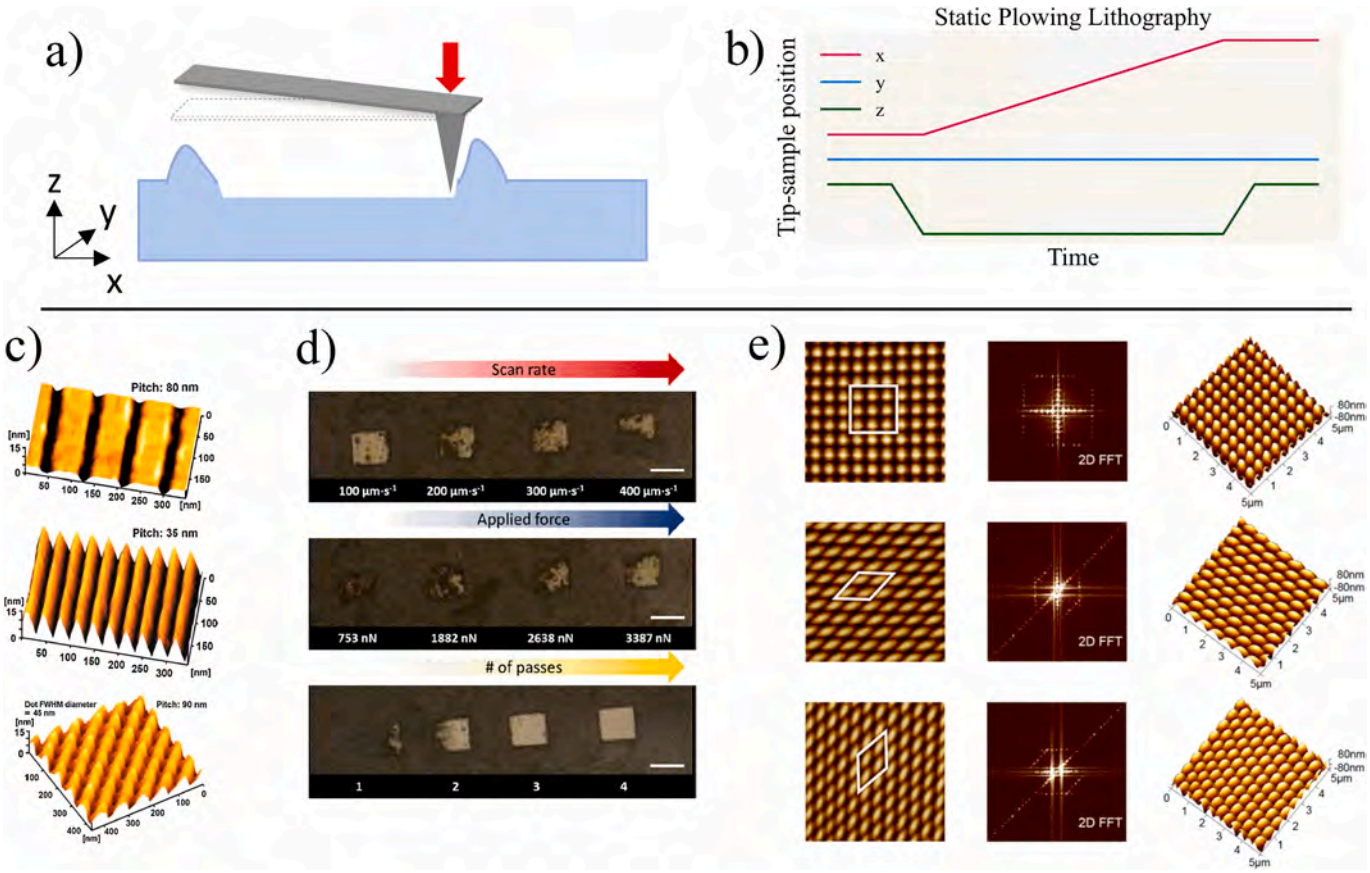

Fig. 3. Static Plowing Lithography technique for the fabrication of complex 2D and 3D nanostructures. (a) Sketch illustration of the SPL technique; the red arrow indicate the constant force acting by the AFM probe on the substrate. (b) Graphical representation of the movement of the AFM probe during SPL in the x ,y, and z planes. (c) From the top to the bottom, 3D AFM topographic images of parallel nanogrooves with a pitch of 80 nm and 35 nm, and quantum dots with a diameter of 45 nm patterned by cross scratching with a pitch of 90 nm. All the nanostructures were scratched by backward direction using diamond-coated tip at contact mode, using a normal force of 9 µN. Reprinted with permission from Ref. [62]. Copyright © 2011 Elsevier B.V. All rights reserved. (d) Optical images showing (50 × 50) μm^2 square micropatterns realized by SPL varying the patterning parameters, such as the tip velocity, the applied force, and the number of scans. All studies were conducted on a $CaCO_3$ nanoparticles (NP) layer. Reprinted with permission from Ref. [67]. Copyright © 2021 American Chemical Society. (e) 2D and 3D AFM images and corresponding 2D FFT images of nanodot arrays patterned by SPL technique. The scratching angles used for the two-step scratching method were 90° and 0°, 90° and 45°, and 0° and 45° (from the to the bottom of the image). Reprinted with permission from Ref. [71]. Copyright 2014 Springer Nature.

drawbacks, the need for an experimental setup more elaborate than the one used for AFM imaging led to the development of the DPL approach, which ensures a pattern almost independent of the scanning direction, and a reduced tip wearing during the nanofabrication process [70]. Y. Yan and coworkers used the Static plowing lithography technique to scratch linear patterns with different orientation, on a polycarbonate (PC) sample surface by means of a diamond probe. In addition, they performed two consecutive tip scans with different scratching angles, in order to obtain complex 3D nanopits arrays. Although this technique is very simple and fast, when operating in contact mode, the presence of cantilever deformation is inevitable as the result of the friction force between the tip and the sample surface. This, in turn, leads to the formation of irregular nanofeatures, with an inhomogeneous profile, severely limiting the use of this technique in the production of nanostructures **(**Fig. 3 **e)**.

As the scratching direction and the tip geometry strongly affect the nanostructures' depth and morphology [62,72], to overcome these drawbacks researchers have developed Dynamic Plowing Lithography (DPL) with which it is possible to generate nanostructures by sculpting the sample surface in semicontact mode [57] **(**Fig. 4 **a and b)**. In DPL, the lateral force is avoided, because the AFM tip is driven to oscillate in the vertical direction at a high frequency while scratching. Besides, the interaction force is relatively small in the dynamic response between the tip and the sample surface, thus only shallow nanostructures can be generated [44,72,73]. In addition, debris from the sculpted substrate could accumulate inside the patterned nanostructures and undesired, remarkably high pile-ups surround the carved structures [57].

Typically, Dynamic Plowing Lithography is performed by setting the AFM in semicontact mode and driving the probe near its resonance frequency above the material to be patterned. The tip oscillates with an amplitude greater than the amplitude usually set for imaging, forcing the probe to strongly interact with the material. For this reason, the force exerted on the material, is not constant but has a period determined by the oscillation frequency of the cantilever. Then, the plastic deformation of the material is mainly determined by the vertical tip's oscillation [72]. Compared to the scratching process of Static Plowing Lithography, the nanostructures fabricated by the Dynamic Plowing Lithography are contoured by pile-ups with heights comparable to that of the structures [57]. Moreover, the formation of chips of the removed material, which is a common drawback when Static Plowing Lithography is employed for patterning metals, does not occur when using DPL [72].

The DPL method is suitable for patterning nanostructures of a few nm on several type of polymers, such as poly(methyl methacrylate) (PMMA) [46,73,75–77], polystyrene (PS) [76], polyimide [78], and poly(3-hexylthiophene) [79]. In this framework, B. Cappella et al. investigated the physical mechanism by which two different polymers, PMMA and PS in particular, could be modified during DPL [76]. It turned out that during the first 20–30 contacts of the tip on a single point of the

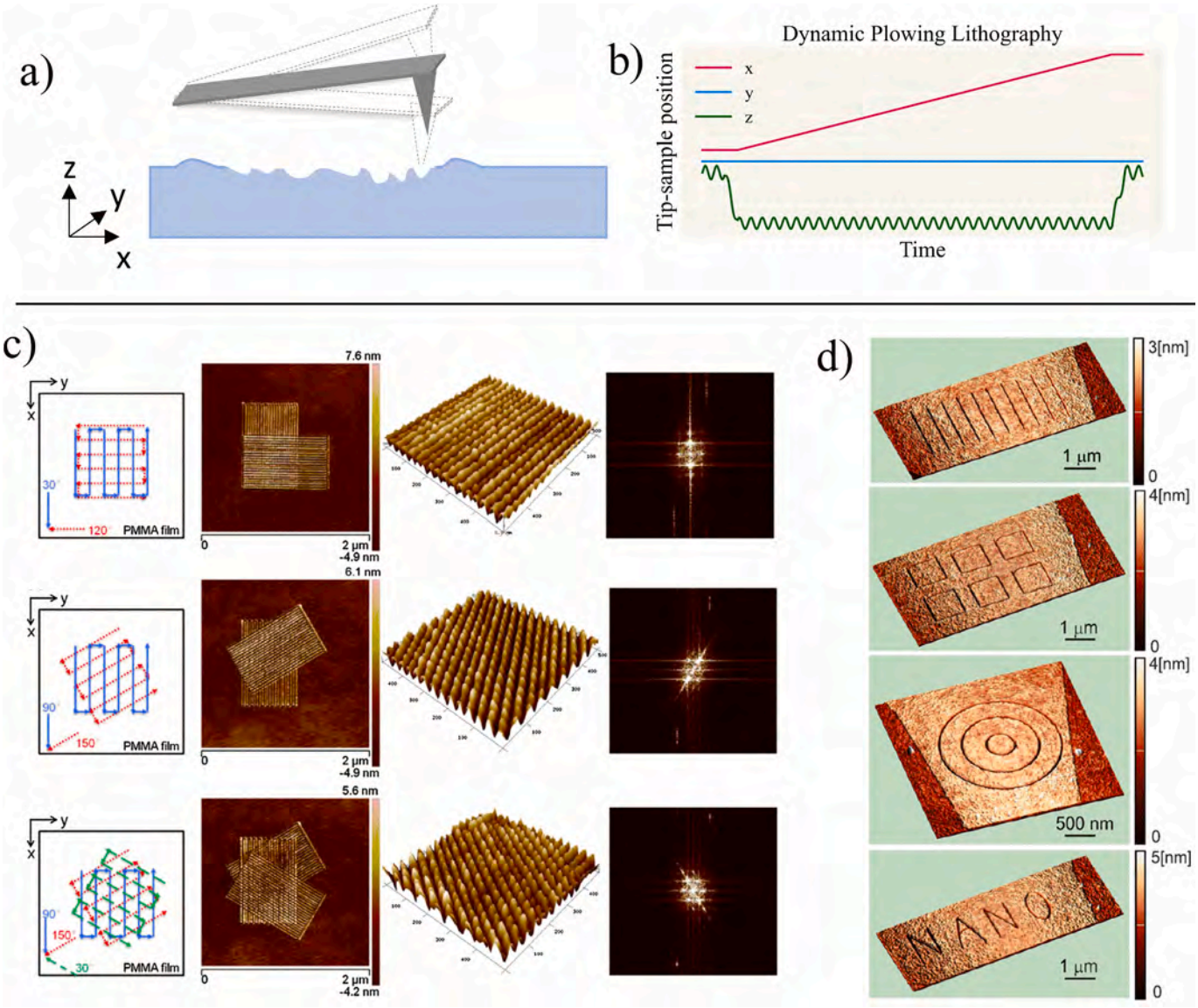

Fig. 4. Dynamic Plowing Lithography technique for the fabrication of nanostructures, nanogrooves, and an array of nanoholes. (a) Illustration of the tip movement and the substrate response during the DPL technique. (b) Graphical representation of the spatial movement of the AFM probe during DPL in the x, y, and z planes. (c) On the left, a schematic representation of the tip movements in the xy plane for the nanopatterning of arrays of nanodots obtained by cross scratching in different tip directions to obtain various array geometries. At the center, 2D and 3D AFM topography images of the nanodots arrays on PMMA. On the right, FFT images obtained from the AFM topography data. Reprinted with permission from Ref. [46]. Copyright© 2017 Elsevier B.V. All rights reserved. (d) 3D AFM topographic images of structures fabricated by DPL on graphene: lines, squares, circles, and the word 'NANO'. Reprinted with permission from Ref. [74]. Copyright © 2013 IOP Publishing Ltd.

sample's surface, the energy dissipated in the process breaks covalent bonds of the polymer chains. A nanohole is progressively carved out during this first step. Then, the successive contacts do not induce the enlargement of the hole, but the displacement of the carved material around the hole to form pile-ups: in this case, the energy is distributed over a larger area and it is insufficient to further break covalent bonds [76].

During the nanopatterning procedure of a single line by DPL, the intermittent contact between the probe and the sample surface can be exploited in two ways: at relatively low scanning rates a single scan can produce a nanogroove, while above a scanning rate threshold, multiple scans can result in equally spaced nanoscale pits [80]. The scanning rate threshold depends on a single parameter, that is the resonance frequency of the cantilever. Y. He et al. employed an AFM equipped with a silicon tip, characterized by a nominal spring constant of 42 N/m and resonant frequency of 320 kHz, to nanopattern array of pits on PMMA [80]. In this case, the authors found that the threshold rate was 100 µm/s and, moreover, the nanoholes' depth was strongly influenced by the scanning rate: as the scanning rate increased, the depth of the patterned nanohole decreased. The relatively high scanning rate resulted in a throughput of 4800 – 5800 pits per second [80]. However, the authors found that the geometry of the nanostructures is also influenced by the scanning direction when an asymmetrical shape tip is used. In a successive paper, the same author explored the possibility to develop a data storage system based on the nanopits' manufacturing by means of the DPL. In this system, the Boolean value "1" was assigned to the patterned nanohole, while the "0" value was assigned to the unpatterned PMMA at an assigned position [81]. The scanning rate was tuned to pattern eight consecutive rods of nanoholes, then 8–bit code words can be read in the normal direction. While the process parameters have been optimized to obtain well-defined rows of equally spaced nanopits, some critical issues still remain, as the non-linearities found in the relationship between the

distance of the nanoholes and the scanning rate and the impossibility of tuning the scanning rate while nanopatterning a single row, that results in a repetition of the pattern [81].

As an alternative to Static Plowing Lithography, the fabrication of nanoholes arrays can be also carried out by crossing two or more arrays of nanogrooves obtained with the DPL technique [62,73]. The main advantage of the use of this approach is the prevention of tip wear because DPL is performed in semicontact mode. However, DPL results are unsuitable for nanopatterning a wide range of materials harder than polymers, due to the weaker interaction with the substrate, if compared to the other mechanical AFM-based nanolithography techniques [73]. In this framework, Y. He et al. investigated the DPL capability to pattern arrays of dots on PMMA by crossing two or three square arrays of nanogrooves, whose pitch (30 nm) corresponds to the distance between two consecutive scanning lines. Checkerboard nanodots were fabricated by cross scratching in the 30° and 120° directions, diamond-shaped nanodots in the 90° and 150° directions, and hexagonal nanodots in the 30°, 90°, and 150° directions. In each pattern, the nanodots' densities orders of magnitude were 10^9 dots per mm^2 [46,73]. The patterned nanogrooves were characterized by a depth of about 2 nm and a width of 15 nm, determined by the tip's apex radius, which was less than 10 nm **(**Fig. 4 **c)**. Moreover, the authors found that the shape of the silicon tip employed in DPL affects the nanostructures' geometry only for scanning directions parallel to or away from the main axis of the rectangular cantilever; in the other cases, the nanostructures are not significantly affected by changing the scanning direction [46] **(**Fig. 4 **c)**.

Although the major efforts to develop the DPL nanopatterning approach have been made on polymeric materials [44], this technique could be interestingly applied to nanostructuring of other specific materials. The manipulation of graphene at the nanoscale, indeed, can take several advantages from the AFM tool. Aiming to a nanolithography technique that does not need the nanofabrication of metallic contacts on the graphene flakes, B. Vasić et al. investigated AFM capability to cut and locally deform the graphene through the DPL setup [74] **(**Fig. 4 **d)**. The DPL test has been performed by a conventional AFM system equipped with a V-shaped cantilever, which presents at its end a tip with a 50–70 nm curvature radius [74]. At first, seven trenches were fabricated side by side, each one was patterned with an increasing interaction force that reached a maximum value of about 68 μN, with which the deeper nanogroove was patterned. The size and depth of the grooves realized by the lowest forces were not measurable because the force applied by the AFM tip was too low to produce an appreciable deformation of the graphene layer, while the other grooves' depth varied from 1 nm to about 4 nm, and their width increased from 40 nm to 50 nm. In addition, those nanostructures were characterized by the presence of a large bulge on the right side. In the last nanogrooves, the graphene layer was cut, displaced, and rolled at the top of the nanostructures by the tip during the DPL process. Where the graphene has been removed, a smooth surface, that widens from the bottom to the top reaching a width of just a few nm, divides the trench from the pristine graphene and represents the underlying SiO_2/Si surface [74]. This experimental setup and the DPL technique enable the realization of more complex nanostructures, such as graphene nanoislands with a diameter of tens of nm, squares, concentric circles, and the word "NANO" (Fig. 4 **d**) [74].

3. Assisted m-SPL techniques

The outstanding performances of AFM, the scientific relevance of the AFM-based analysis, its capability to be used as a nanofabrication tool, and, above all, its relatively simple operating principle, paved the way for the development of several m-SPL variants. In this frame, further energy sources were added to the conventional AFM-based nanofabrication approaches to facilitate and improve the mechanical removal of material. Through the integration of additional hardware components to the conventional experimental setup, mechanical, thermal, or electric energy forms can be provided to the AFM system, improving the efficiency of the lithography process and the quality of the final result. To this aim, different approaches have been explored during the last decades and they are presented in this section.

3.1. Vibrating assisted m-SPL

As described in the previous section, the DPL is based on the AFM tapping mode, in which the probe oscillates close to its resonant frequency. The choice of this specific frequency makes the oscillation amplitude of the probe very sensitive to the interaction between the tip and the material and, therefore, to the variation of the distance gap between the tip and the sample surface. Although this represents an enormous advantage when performing AFM imaging of soft material, such as topography and phase shift detection, in the case of DPL this circumstance represents a disadvantage as the sensitivity of the system limits the capability to optimize the geometric characteristics and the uniformity of the nanostructures [82].

To overcome these drawbacks, L. Zhang and J. Dong developed the Ultrasonic Vibration Assisted Atomic Force Microscopy (UVA AFM) nanomachining technique [82,85]. In this approach, the tip is set to oscillate in the vertical direction at an ultrasonic frequency (f), which is much higher than the resonant one (f_r, with $f \gg f_r$); moreover, a high frequency circular planar motion between the tip and the sample is added to the nanofabrication system, in order to achieve better control over the nanofabrication process and, then, to increase the material removal rate [82]. Indeed, when the cantilever vibrates at a frequency below the resonant frequency ($f < f_r$), the probe's oscillations follow the sample's motion, and no significant indentation is made. However, at ultrasonic frequency, the cantilever's dynamic stiffness increases as the cube of the frequency, so the tip indents into relatively soft materials [82,85].

To demonstrate the effectiveness of UVA AFM, a few nanometers deep trenches have been fabricated on both aluminum and PMMA layers by means of a silicon probe set to oscillate in the vertical direction with an ultrasonic frequency of 3 MHz. In addition, a circular motion at a frequency of 4 kHz in the plane of the sample was applied. In order to study the lateral force signal and friction, the cantilever's deflection was accurately recorded [85]. In UVA AFM, the depth of the nanopatterned features is mainly controlled by the oscillation amplitude of the cantilever. As for other AFM-based nanofabrication techniques, the nanostructures are contoured by the material removed during the nanomachining process [85] which strongly limited the use of the nanopatterned nanostructures. Anyway, the application of smaller interaction forces than the other AFM-based nanofabrication techniques (i.e. Static Plowing Lithography) allows to prevent the tip wear during the lithography process [82,85]. J. Deng, J. Dong and P. Cohen used UVA-AFM to successfully realize complex nanostructure with discrete height levels and continuous changes on a thin PMMA layer **(**Fig. 5 **c)**. Moreover, the authors explored the capability of transferring the complex, 3D nanostructures from polymer layer onto the underling silicon substrate by RIE process [83].

In another research work, J. Deng and co-workers used the UVA-AFM for realization of 3D microstructures on PMMA, further used as the master in the 3D NIL **(**Fig. 5 **d)** [84]. A mathematical model for UVA AFM lithography was developed by Shi et al. to determine a relation that estimates the ultrasonic machined depth based on the tip oscillation amplitude [86]. The theoretical representation of the system was fronted according to the equivalent point-mass model of the continuous AFM probe [87], and applying an approximation for high-frequency to the Euler-Bernoulli beam theory [86,88]. The results of the simulations were compatible with experimental data that were collected after machining nanogrooves on a 5 nm thin film of PS. In particular, the UVA AFM tool was capable of regulating the machining depth at approximately 0.15 nm by controlling the probe oscillation amplitude [86]. The theoretical model was further analyzed to determine the phase change when the tip

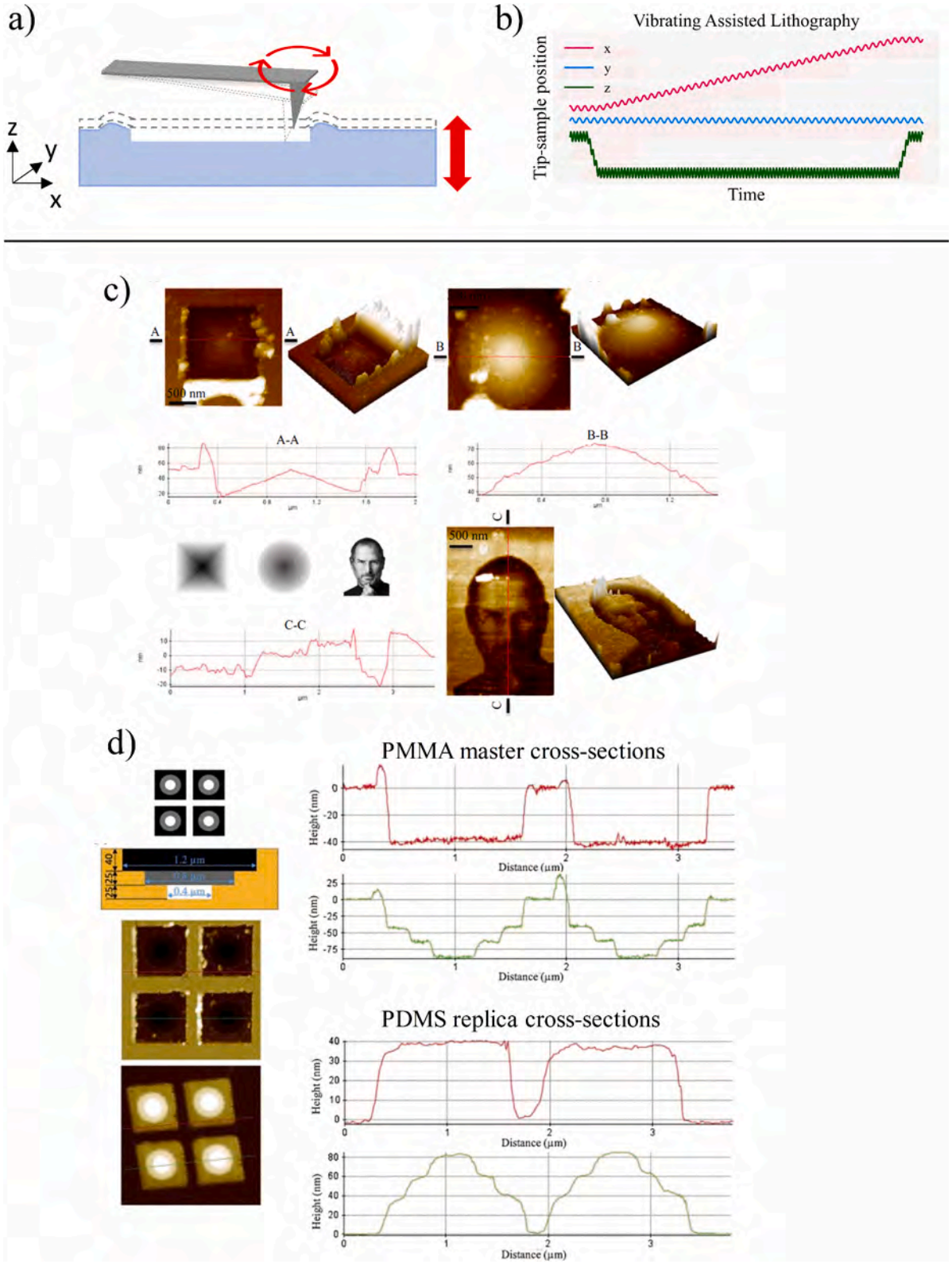

Fig. 5. Vibrating assisted m-SPL technique for complex 3D micro- and nano-structures fabrication. (a) Schematic representation of Vibrating assisted m-SPL, depicting the circular movement of the AFM probe and the substrate vibration. (b) Graphical representation of the AFM probe spatial movement during the vibrating assisted m-SPL in the x ,y, and z directions. (c) 2D and 3D view of AFM characterization of pyramidal-shaped nanostructures and their cross section. On the bottom side, bitmap images of pyramid, cone and AFM 2D and 3D view of Steve Jobs' profile. Reprinted with permission from Ref. [83]. Copyright: The Authors. Published by Elsevier B.V. (d) On the left side, schemes in grayscale of 3D nanopatterns and feature dimensions of each nanopatterns (the height unit on the left side of the image is nanometers). PMMA master template realized by Vibrating assisted m-SPL, and its cross-sectional profiles on the right. PDMS mold reversely casted by using the PMMA master template, and its cross-sectional profiles on the right side. Reprinted with permission from Ref. [84]. Copyright © 2021 Elsevier B.V..

reaches the interface of an ultra-thin film, then it was tested by monitoring in real-time the nanopatterning of the interface between a thin film of PS on Si [89]. The change in the slope of the depth and phase data trend, that were collected for nanogrooves machined on an 11 nm thick PS thin-film, is consistent with the numerical simulation of the mathematical model [89].

To better understand the role of debris in the machining process, a similar experimental setup and a proper theoretical model were developed. The AFM phase response can sense the effect of the debris on machined depth, even if the debris formation is random and unpredictable [90].

During multiple studies, Deng et al. developed and improved the UVA AFM 3D nanofabrication of structures on PMMA and successfully applied this technique in the fabrication of 3D master nanotemplates for 3D soft lithography [83,84,91–95]. Essentially, UVA AFM technique allows two approaches for 3D nanopatterning: layer-by-layer machining and varying the set point of the normal force applied during machining. In layer-by-layer machining, the whole nanostructure is fabricated by machining several layers one by one but changing the patterns for each layer [91]. The layer-by-layer machining approach was employed in the realization of simple features on PMMA, as stair-like nanostructure with five steps. Moreover, complex nanostructure with discrete and continuous height changes were successfully fabricated in raster scan mode from bitmap images [83,93].

3.2. Nanomilling

As described in the last section, in the UVA AFM the tip motion relative to the sample's surface consists of two main movements: the vertical vibration of the tip at an ultrasonic frequency, and a circular, in-plane motion [82]. For UVA AFM, the main characteristic innovation could be addressed in the first one of these motions. Indeed, the capability of the in-plane circular motion to improve the nanostructures' quality has been investigated by B. A. Gozen and O. B. Ozdoganlar in 2010, and it led to the development of a different lithography technique called nanomilling [96]. Moreover, both these approaches rely on an AFM system equipped with a three-axis piezoelectric actuator [97] that allows the supply of out-of-phase sinusoidal excitations in mutually perpendicular directions to obtain the circular motion of the tip relative to the sample [96,97]. Nanomilling was performed by using two different tip circular movements: a trajectory parallel to the plane of the sample's surface, called in-plane motion, and one perpendicular to it, named out-of-plane motion [96] **(**Fig. 6 **a and b)**. Although both the basic configurations are effective in nanopattering, the in-plane configuration was taken into more consideration because of its ability to pattern different materials with high resolution [98,99]. The

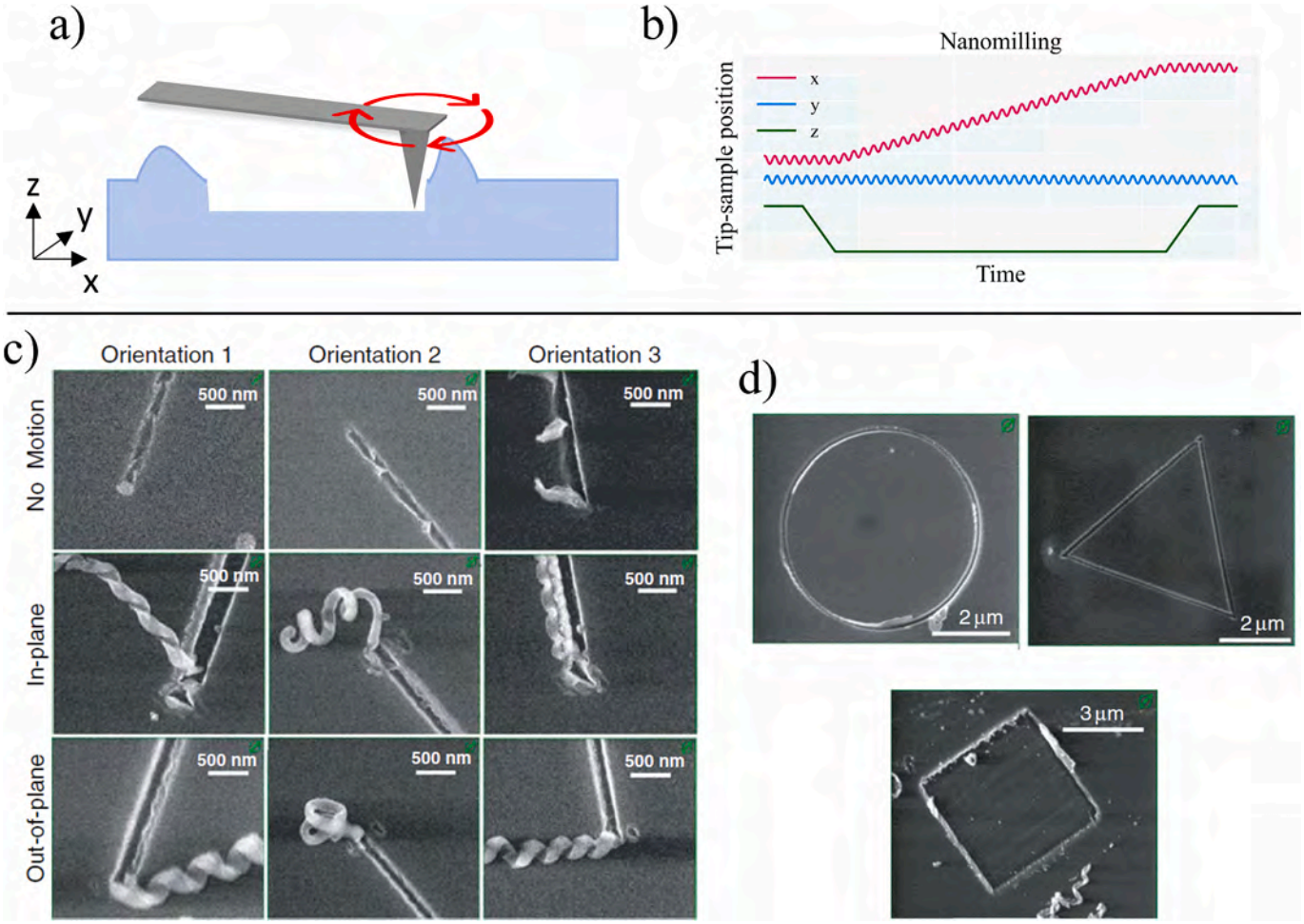

Fig. 6. Nanomilling AFM-based Lithography technique for the fabrication of nanochannels. (a) Illustration of the tip movement on the substrate during the nanomilling technique; the circular motion of the tip is represented by the red arrows. (b) Graphical representation of the spatial movement of the AFM probe in the x ,y, and z directions during nanomilling procedure. (c) SEM images of the channels created using different nanotool motions. The material removal mechanism is shearing dominated, as testified by the presence of long and curled chips, that are observed for the cases with nanotool motions. Reprinted with permission from Ref. [96]. The Author(s) 2010. This article is published with open access at Springerlink. (d) The nanochannels can be shaped into different planar geometries by the proper rotation of the substrate. Reprinted with permission from Ref. [96]. The Author(s) 2010. This article is published with open access at Springerlink.

material-removing mechanism results from the combination of the circular movement with the motion along the feeding direction at a prescribed depth resulting in the material-removing process [96].

B. Arda Gozen and O. Burak Ozdoganlar used AFM nanomilling for the realization of channels with a length of 5 μm and 100 nm depth by using each of the in-plane and out-of-plane configurations on SU-98 resist (Fig. 6 **c)** [96]. After this preliminary optimization step, the authors realized complex 3D nanostructures, such as circular, triangular and square nanostructures by both in-plane and out-of-plane configurations (Fig. 6 **d)** [96].

AFM equipped with silicon or diamond probes has been suitable for patterning 2D/3D nanostructures on polymeric materials, such as PMMA [97,100,101], metals like copper [98,102,103], aluminum alloys [99], silicon [98,104], and other customed materials [105]. A typical characteristic that is found in nanomilling is the formation of chips of the removed material rather than pile-ups or debris; as a consequence, the edges of nanogrooves and other nanostructures patterned by this technique are well defined compared to the conventional AFM scratching approach [96]. Moreover, the machined nanotrenches width can be easily tuned by setting the maximum amplitude of the driving voltage that determines the diameter of the circular trajectory, allowing to fabricate a nanogroove of chosen dimensions in a single pass, regardless of the tip radius [96].

The relevance of this technique was proven by a deep study of the wearing of ultrananocrystalline diamond (UNCD) AFM tips when nanomilling silicon and copper [98]. The tip was set to rotate in-plane with a frequency of 4 kHz and a radius of 100 nm. Trenches of an expected depth of 150 nm were patterned on {1 0 0}-silicon along the ⟨1 1 0⟩ direction, and on copper. The tip wearing was monitored by measuring the probe's topography at different stages of the nanofabrication process, corresponding to increasing patterned length. This experiment shows how the tip undergoes rapid wear during the first mm for silicon, and 40 mm for copper, then it reaches a steady-state wear phase, where the wear rates are reduced to a relatively constant value measured to be 0.135 nm/mm for copper, and 0.19 nm/mm for silicon [98].

The nanomilling approach has been validated by the modeling of the technique [99–101] and Molecular Dynamics (MD) simulations [102–104], that accounted for the tip geometry and trajectory in the manufacturing of different materials. Due to the cyclic tip trajectory, two scratching processes could be distinguished in a single loop: the tip cuts the pristine material along the scanning direction, thus creating the outer profile of the nanostructures; during the remaining part of the trajectory, the tip avoids the untouched material and refines the inner part of the nanostructures, enhancing their depth [101]. The direction of rotation of the tip, which can be clockwise or counterclockwise, as well as its geometry, determines the chip formation and affects the nanostructures' morphology [100,101,104].

J. Wang et al. established a theoretical model to predict the machined depth of nanochannel manufactured on single-crystal silicon by implementing the AFM nanomilling technique and using a triangular pyramidal diamond tip [106]. The model was tested, and the system parameters, including the feeding direction and the crystal orientation of the sample, were optimized to fabricate well-defined nanochannels. The nanostructures were characterized by means of Raman Spectroscopy and.

Transmission Electron Microscopy (TEM) to determine how the nanofabrication process affects the crystallographic order of silicon: stacking faults, dislocations, and other atomic-scale defects occur at the interface between the bulk material and the surface that has been exposed to the high pressure and shear stress [106].

Nanomilling has been successfully employed in the nanopatterning of multi-layer metallic film [105] and in the manufacturing of 3D nanostructures by the modulation of the normal force applied during the process [99]. Moreover, the chip formation represents an advantage for debris removing and after process treatments, because easy and effective removal strategies could be adopted, while these are not suitable for the elimination of debris and pile-ups formed in conventional scratching methods [99].

3.3. Thermal-assisted SPL material removal

A particular variant of Scanning Probe Lithography (SPL), known as thermal Scanning Probe Lithography (t-SPL), has recently regained prominence due to its speed and reliability. In this method, localized material modifications are induced using thermal energy generated by a heated tip (Fig. 7 **a and b)**. Indeed, the AFM probe can be heated up to 800 °C by employing a laser beam [41,107,108] or a micrometric electric resistance [41,109]. In this way, the tip represents a heat source that can be used in different applications, such as improving the material removal in mechanical fabrication processes, the determination of a local chemical change of the 2D material substrates, and the transfer of material to the sample's surface through a physic or chemical process thermally activated. The tip heating is achieved through the current flow in a specially shaped cantilever, usually composed of doped single-crystal silicon [110], low-doped Si [111–113], or a combination of highly doped conductive cantilever with a low-doped region at the top, where the tip is located [114]. The cantilever can be represented as a conductive resistive element, which allows the application of a voltage and the resistive tip heating through the Joule effect [114]. t-SPL has proved to successfully nanopattern different materials, i.e. pentaerythritol tetranitrate (PETN) [110], PMMA [115], Molecular Glass (MG) photoresists [111,116,117], and poly(phthalaldehyde) (PPA) [118,119].

Generally speaking, t-SPL techniques were categorized into the removal, conversion, and addition of material. The main application of t-SPL involves localized material removal using a heated tip to alter the surface topography. Two distinct processes are employed: mass-preserving thermomechanical indentation, where the material is displaced to the sides of each indentation, and permanent removal of material from the surface through sublimation. The latter is a captivating process with which it is possible to remove material by sublimation: in this case, the high-temperature tip causes the activation of a chemical reaction that has gaseous products, so the material can be removed without leaving any residual debris on the sample [116].

Nonetheless, this section is focused on the mass-preserving thermomechanical indentation method, in which the m-SPL techniques are coupled with a high-temperature heated tip. Polymers are particularly suitable materials to exploit in this method because of their physicochemical properties, i.e. the glass transition, or the enhancement of chemical reactivity at high temperatures. The coupling of high temperature with the application of mechanical force leads to an increase in the efficiency of the material removal process and the improvement of the quality of the patterned nanostructures is achieved.

Recently, S. Chang and colleagues used the t-SPL technique with the aim of manipulating a polymethyl methacrylate thin film at the nanoscale through a single scratch. The authors conducted a systematic analysis on the correlation between machining performance and scratching velocity, considering variable tip thermal conditions while maintaining a uniform normal force. Moreover, the theoretical framework of stick–slip friction was applied to rationalize the genesis of nanopit architectures (Fig. 7 **c**) [120].

O. Coulembier and co-workers exploited t-SPL to pattern large areas of a polymeric film with high throughput and resolution. The t-SPL method is showcased through a debris-free polymer decomposition reaction activated by the close proximity of a heated probe (Fig. 7 **d)** [118].

Y. K. R. Cho et al. methodically investigated the t-SPL nanofabrication parameters to improve the technique's resolution. Silicon cantilevers were employed to pattern nanogrooves on a 6–7 nm thick layer of PPA on a silicon substrate [121]. The temperature of the resistive heater in correspondence with the tip was studied in the range from

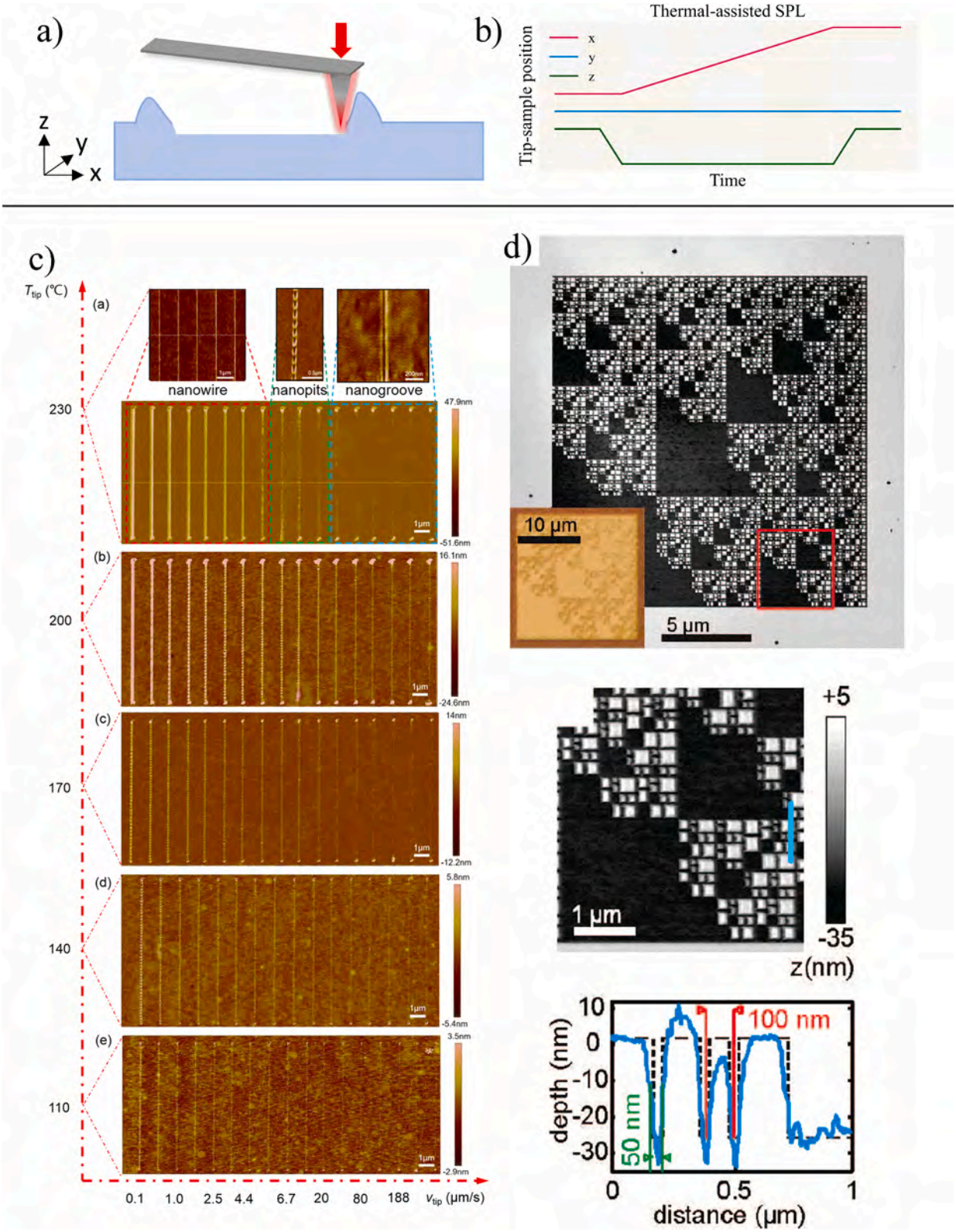

Fig. 7. Thermal-assisted SPL technique. (a) Sketch representation of the Thermal-assisted SPL nanofabrication method and (b) graphic describing the spatial movement of the AFM probe in the x ,y, and z directions during procedure thermal-assisted SPL technique. The red arrow indicates the force applied by the tip to the sample surface while the red shadow around the AFM tip represents the increase of the tip temperature. (c) AFM characterization of 10 μm long nanogrooves arrays obtained by thermomechanical nanolithography under different coupling of tip temperature (T_{tip}) and velocity (v_{tip}) on PMMA. In details, the v_{tip} values were set to 0.1, 0.5, 1.0, 1.7, 2.5, 3.4, 4.4, 5.5, 6.7, 8, 20, 40, 80, 128, 188, 260, and 500 μm/s (from left to right in AFM images) while the T_{tip} was 110, 140, 170, 200, and 230 °C while the normal force applied was kept constant and equal to 250 nN. Reprinted with permission from Ref. [120]. Copyright © 2021 The Author(s). Published by Elsevier Ltd. (d) AFM acquisition of a patterned (18 × 18) μm^2 area by means of thermal-assisted SPL technique. Inset bottom left of the image on the top: optical image of the nanopatterned area. On the right side, close-up view of the sample area highlighted with a red box in the AFM image and cross-section profile (blue line) taken along blue cross section line in image above. Reprinted with permission from Ref. [118]. Copyright © 2009 American Chemical Society.

525 °C to 800 °C in steps of 25 °C, and for each temperature, the effect of the normal force applied was studied from 0 nN to 30 nN. The tip radius at the apex was about 3 nm, and the best results have been obtained with a temperature of approximately 600 °C [121]. After the t-SPL nanopatterning, the nanogrooves were transferred on the underlying silicon layer by a dry-etching process. The optimization of parameters has made possible the nanofabrication of 14 nm half-pitch lines in silicon with a feature size of 7 nm [121].

Moreover, a paper by P. Vettiger et al. [122] demonstrated that the development of a system composed of thousands of probes operating in parallel for nanofabrication or imaging was possible. In particular, they fabricated an array of 32 × 32 AFM probes that was capable of parallel t-SPL nanoindentation on PMMA. This system was developed by IBM company for high-density memory Storage and reading [122].

To conclude, this nanofabrication technique has significant potential and has recently been applied to overcome the limitations of conventional techniques for the realization of components that can be integrated into the next generations of technological devices. Relevant examples of these components are optical Fourier surfaces for optical devices [123], metal contacts fabricated on monolayer MoS_2 exhibiting vanishing Schottky barriers for top-gate and back-gate field-effect transistors [124], and nanopatterned biocompatible silk fibroin to control the growth of conductive filaments for the implementation of reliable and ultrafast memristors [125].

3.4. Bias-assisted m-SPL

According to specific characterization techniques such as Kelvin probe force microscopy (KPFM) and Electric Force Microscopy (EFM) [126], conductive tips can be used to study the electric properties of the sample's surface by setting a proper electric potential. The application of an electric potential between the tip and metallic, conductive sample surface was further exploited to develop other AFM-based nanolithography techniques **(**Fig. 8 **a and b)** [42]. Overviewing those different approaches, deposition techniques in gaseous or liquid environments have been developed from the capability to control electrochemical reactions in the proximity of the tip, and these approaches go under the name of Local Anodic Oxidation (LAO) [127,128,129]. LAO allows the manufacturing of nanostructures, oxides for example, on different materials, such as silicon [128,129], Diamond-like Carbon (DLC) film [129], and graphite [130]. On the other hand, AFM Electrochemical Nanomachining (ECM) was used to directly nanopatterning, surface planarizing, and fabricating of 3D-ECM. The key point of ECM is to confine electrochemical reactions at the micro/nanometer scale. For example, Bark et al. carried out the lithography of line patterns of various widths and thicknesses on NbS_2 thin films with ECM by varying scan speed and applied voltage.

G. Lee et al. have explored the advantages of activating electrochemical reactions through ultra-short potential pulses during a mechanical scratching nanofabrication process on Cu [131]. The conductive probe was immersed in an electrolyte solution, obtained by combining $HClO_4$ 0.1 mM and $CuSO_4$ 0.01 mM. The sign and magnitude of the potential difference between the tip and the sample, the duration and frequency of the potential pulses, as well as the scanning speed of the tip on the sample influenced the deposition rate of copper from the sample to the tip or *vice versa* [131]. For this reason, the shape of the structures depends on the scratching and biasing voltage pulse parameters, and nanogrooves can appear surrounded by pile-ups or not, based on the pulse amplitude. In particular, the width of the nanogrooves tends to be almost proportional to the pulse amplitude and duration, and inversely proportional to the tip scanning rate [131] **(**Fig. 8 **c)**.

Similarly, Y. Yang and W. Zhao investigated the effects of coupling the AFM scratching method with a voltage bias between the tip and a sample made of a thin film of copper to manufacture 2.5 D nanostructures [42]. To better understand the effects of coupling, the same nanostructures were first patterned with an unbiased tip, i.e. purely mechanical scratching, and, successively, the same structures were patterned with the biased tip alone, without applying any normal force on the sample [42]. This study demonstrates that the 2.5D nanostructures machined on copper by the coupling AFM lithography were deeper and smoother with respect to the ones patterned by the AFM mechanical lithography and the AFM electric lithography. Moreover, the authors demonstrated the existence of a potential threshold for copper, beyond which material removal processes are activated due to the presence of an electric discharge, resulting in a shock wave and local heating of the sample where the tip is located. Moreover, this strategy was successful for the nanopatterning of platinum, while the mechanical scratching alone failed [42] **(**Fig. 8 **d)**.

4. Challenges and perspectives

In this review, we reported the state of the art of the mechanical–Scanning Probe-based Lithography techniques, describing in-depth their main advantages and disadvantages, together with their practical applications in several nanotechnology fields and future perspectives.

First, AFM provides high-resolution imaging and manipulation capabilities at the nanoscale, enabling the creation of intricate nanostructures with unprecedented precision. Its versatility allows for application across various materials, including metals, semiconductors, and polymers. Additionally, AFM enables non-destructive imaging of surfaces with atomic or near-atomic resolution, crucial for characterizing surfaces before and after nanolithography.

Moreover, AFM-based mechanical lithography allows for direct-write capabilities, facilitating precise removal of material at the nanoscale. Real-time monitoring during the fabrication process ensures a better understanding of the physical phenomena involved in the nanolithography process, allowing the comparison of experimental data with theoretical models of m-SPL.

At first, we focused on the simplest mechanical AFM-based method, i.e. nanoindentation, with which it is possible to realize a single or arrays of nanoholes on the substrate surface. Those nanoholes could be transferred on a more resilient substrate *via* etching processes or they can act as a mask for the deposition of metallic nanodisks. Successively, we described the Pulse-Atomic Force Lithography which is regarded as the evolution of the nanoindentation method. Indeed, by the overlapping of single indentation it is possible to pattern 2D and 3D nanostructures with constant and varying depth profiles. After that, we report AFM Static and Dynamic Plowing lithography techniques, directly developed from Contact and Semicontact AFM imaging modes, respectively. In particular, Static Plowing Lithography involves a stationary probe scratching the material surface to create nanoscale patterns. On the other hand, Dynamic Plowing Lithography, uses an oscillating probe to induce controlled deformation and material removal, allowing for precise nanostructuring. Finally, we focused on the m-SPL coupled with additional energy sources such as vibration (UVA AFM and Nanomilling), high temperature (t-SPL), and voltage (Bias-assisted SPL). More in details, thermal SPL allows for controlled heating to manipulate material properties. Bias-assisted lithography utilizes voltage application for precise modification of surfaces. Ultrasonic vibration in nanomilling with AFM enables efficient material removal, expanding the versatility of nanofabrication processes. These combined techniques offer a synergistic approach, providing greater flexibility and control in creating nanostructures for various applications.

Several key considerations should be made in developing a practical and concrete use of m-SPL techniques. The most important aspect that must be taken into account includes ensuring the reliability of the tip for patterning extensive geometries without wear or breakage, which would otherwise compromise the correct realization of the nanostructures.

Another concern emerges if the efficiency of the single-tip AFM system to pattern large areas (of the order of cm^2) is compared to conventional maskless techniques like EBL, FIB, and TPL. Indeed, m-SPL offers several advantages, such as the low cost of the nanofabrication

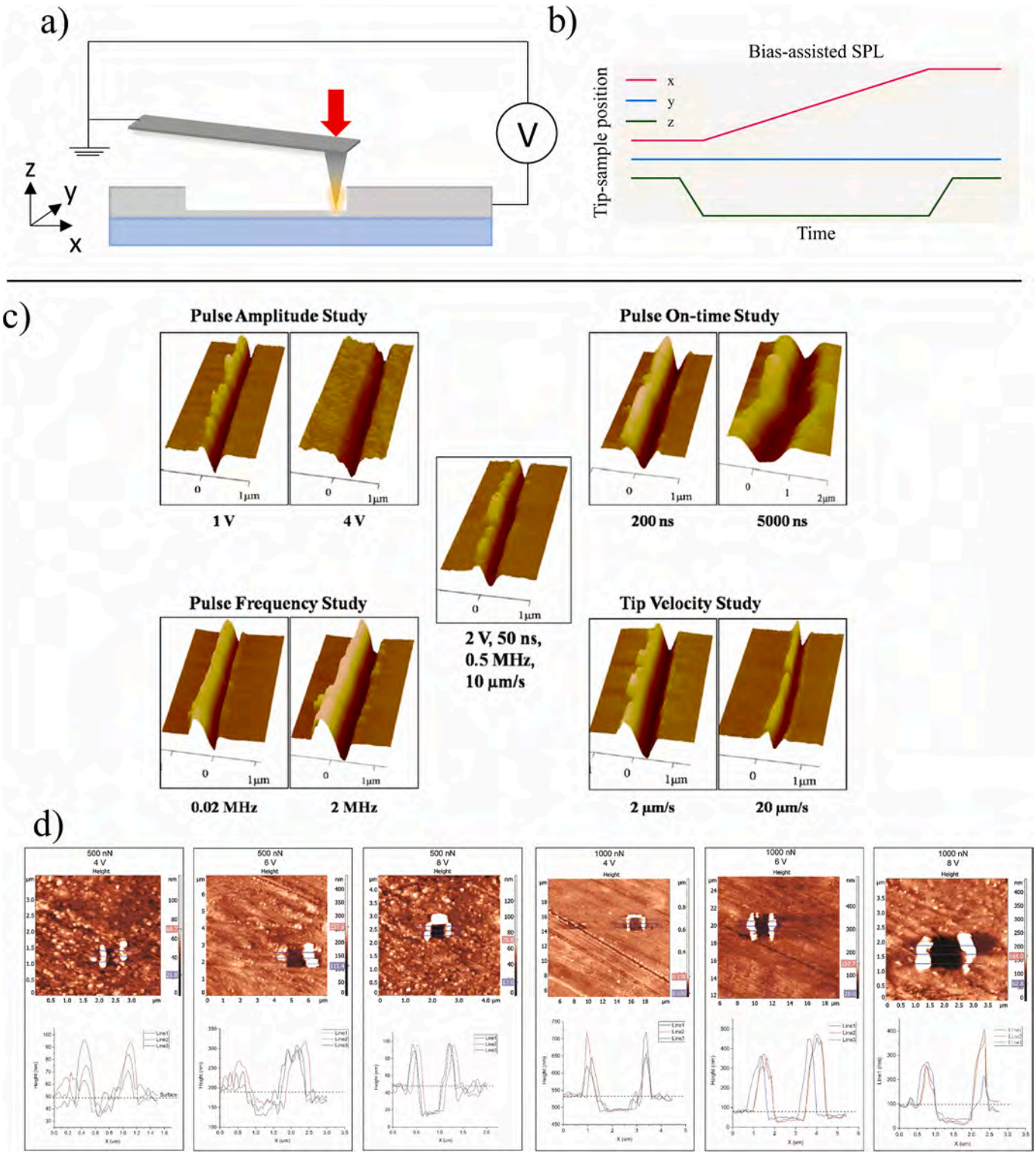

Fig. 8. Bias-assisted m-SPL technique. (a) Sketch representation of the Bias-assisted m-SPL and (b) graph depicting the spatial movement of the AFM probe in the x , y, and z directions during the Bias-assisted m-SPL procedure. The red arrow in (a) indicates the force applied by the tip during the lithography while the yellow sign around the AFM tip represents the bias voltage. (c) AFM 3D topography images of the study of nanochannels patterned by changing the electrical pulse parameters and the tip velocity. At center, nanogroove fabricated by applying a pulse amplitude of −2 V between the tip and the sample, on-time of 50 ns, at a frequency of 0.5 MHz, and a tip velocity of 10 µm/s; The other topography images illustrated the effect of changing one parameter with respect to the central one. Reprinted with permission from Ref. [131]. Copyright © 2010 IOP Publishing Ltd. (d) AFM topography images of the square patterns realized by coupling AFM lithography on the Cu thin film surface and the corresponding cross sections. From left to right, the first tree squares were sculpted with a force equal to 500 nN and the applied voltage was set to 4, 6, and 8 V while the last tree squares were patterned with an higher force (1000 nm) and a voltage of 4, 6, and 8 V. Reprinted with permission from Ref. [42]. Copyright © 2019 The Society of Manufacturing Engineers. Published by Elsevier Ltd. All rights reserved.

apparatus, the capability to perform the nanofabrication at ambient conditions, the nanometric resolution achievable in the nanopatterning processes, the non-negligible possibility to image the nanostructures after their nanopatterning with the same instrument, and the reduction in the post-processing steps. In addition, the level of detail obtained in the nanostructures presented in this work is difficult to reach with sophisticated conventional techniques like EBL and even unlikely with techniques of easy implementation, such as photolithography and NIL. Moreover, the development of new m-SPL techniques, the possibility of coupling the mechanical action of the process with other energy sources, and their continuous optimization enhance the m-SPL versatility. In this context, the selection of the most suitable m-SPL technique for a specific application largely depends on the characteristics of the material to be patterned and on the desired level of resolution. Moreover, further advancements in multifunctional materials manipulation may lead to integrated nanoscale devices. Additionally, the development of systems using thousands of tips for parallel operations may offer the most promising path for integrating m-SPL techniques into industrial processes. To sum up, improving 3D nanofabrication capabilities and increasing throughput could expand AFM applications in both scientific research and industrial fields. Continued research may also uncover new applications in fields like nanoelectronics, photonics, and biotechnology, further broadening the impact of AFM.

CRediT authorship contribution statement

Lorenzo Vincenti: Writing – review & editing, Writing – original draft, Methodology, Investigation, Conceptualization. **Paolo Pellegrino:** Writing – review & editing, Writing – original draft, Visualization. **Mariafrancesca Cascione:** Writing – review & editing. **Valeria De Matteis:** Writing – review & editing, Conceptualization. **Isabella Farella:** Writing – review & editing. **Fabio Quaranta:** Writing – review & editing. **Rosaria Rinaldi:** Writing – review & editing, Supervision, Resources.

Declaration of competing interest

The authors declare that they have no known competing financial interests or personal relationships that could have appeared to influence the work reported in this paper.

Data availability

No data was used for the research described in the article.

Acknowledgments

I. Farella acknowledges funding PNRR MUR project PE0000023-NQSTI financed by the European Union – Next Generation EU.

References

[1] H. Rauscher, B. Sokull-Klüttgen, H. Stamm, The European Commission's recommendation on the definition of nanomaterial makes an impact, Nanotoxicology 7 (7) (2012) 1195–1197, https://doi.org/10.3109/17435390.2012.724724.
[2] M.F. Hochella, et al., Natural, incidental, and engineered nanomaterials and their impacts on the Earth system, Science 363 (6434) (2019) eaau8299, https://doi.org/10.1126/science.aau8299.
[3] S. Bayda, M. Adeel, T. Tuccinardi, M. Cordani, F. Rizzolio, The history of nanoscience and nanotechnology: from chemical-physical applications to nanomedicine, Molecules 25 (1) (2019) 112, https://doi.org/10.3390/molecules25010112.
[4] J.O. Cross, R.L. Opila, I.W. Boyd, E.N. Kaufmann, Materials characterization and the evolution of materials, MRS Bull. 40 (12) (2015) 1019–1034, https://doi.org/10.1557/mrs.2015.271.
[5] C. Yugma, J. Blue, S. Dauzère-Pérès, A. Obeid, Integration of scheduling and advanced process control in semiconductor manufacturing: review and outlook, J Sched 18 (2) (2015) 195–205, https://doi.org/10.1007/s10951-014-0381-1.
[6] L. Chen, et al., Millifluidics, microfluidics, and nanofluidics: manipulating fluids at varying length scales, Mater. Today Nano 16 (2021) 100136, https://doi.org/10.1016/j.mtnano.2021.100136.
[7] Y. Xu, Nanofluidics: A new arena for materials science, Adv. Mater. 30 (3) (2018) 1702419, https://doi.org/10.1002/adma.201702419.
[8] F. Hui, M. Lanza, Scanning probe microscopy for advanced nanoelectronics, Nat Electron 2 (6) (2019) 221–229, https://doi.org/10.1038/s41928-019-0264-8.
[9] S.A. Jasim, et al., Molecular Junctions: introduction and physical foundations, nanoelectrical conductivity and electronic structure and charge transfer in organic molecular junctions, Braz J Phys 52 (2) (2022) 31, https://doi.org/10.1007/s13538-021-01033-z.
[10] L. Hui, R. Bai, H. Liu, DNA-based nanofabrication for nanoelectronics, Adv Funct Materials 32 (16) (2022), https://doi.org/10.1002/adfm.202112331. Art. no. 16.
[11] J. Kim, et al., Fabrication of plasmonic arrays of nanodisks and nanotriangles by nanotip indentation lithography and their optical properties, Nanoscale 13 (8) (2021) 4475–4484, https://doi.org/10.1039/D0NR08398D.
[12] S. Tarantino, A.P. Caricato, R. Pelle, C. Capomolla, V. De Matteis, Cancer treatment using different shapes of gold-based nanomaterials in combination with conventional physical techniques, Pharmaceutics 15 (2) (2023) 500, https://doi.org/10.3390/pharmaceutics15020500.
[13] F. Moradi Kashkooli, M. Soltani, M. Souri, Controlled anti-cancer drug release through advanced nano-drug delivery systems: Static and dynamic targeting strategies, J. Controlled Release 327 (2020) 316–349, https://doi.org/10.1016/j.jconrel.2020.08.012.
[14] R. Nagraik, A. Sharma, D. Kumar, S. Mukherjee, F. Sen, A.P. Kumar, Amalgamation of biosensors and nanotechnology in disease diagnosis: Mini-review, Sensors Internat. 2 (2021) 100089, https://doi.org/10.1016/j.sintl.2021.100089.
[15] P. Erkoc, F. Ulucan-Karnak, Nanotechnology-based antimicrobial and antiviral surface coating strategies, Prosthesis 3 (1) (2021) 25–52, https://doi.org/10.3390/prosthesis3010005.
[16] J. Oh, et al., Cicada-inspired self-cleaning superhydrophobic surfaces, J. Heat Transfer 141 (10) (2019) 100905, https://doi.org/10.1115/1.4044677.
[17] G. Funda *et al.*, "Nanotechnology Scaffolds for Alveolar Bone Regeneration," *Materials*, 13(1), , 2020, doi: 10.3390/ma13010201. 201.
[18] Z. Ye, et al., Laser nano-technology of light materials: Precision and opportunity, Opt. Laser Technol. 139 (2021) 106988, https://doi.org/10.1016/j.optlastec.2021.106988.
[19] B.D. Gates, Q. Xu, M. Stewart, D. Ryan, C.G. Willson, G.M. Whitesides, New approaches to nanofabrication: molding, printing, and other techniques, Chem. Rev. 105 (4) (2005) 1171–1196, https://doi.org/10.1021/cr030076o.
[20] A. Biswas, I.S. Bayer, A.S. Biris, T. Wang, E. Dervishi, F. Faupel, Advances in top–down and bottom–up surface nanofabrication: Techniques, applications & future prospects, Adv. Colloid Interface Sci. 170 (1–2) (2012) 2–27, https://doi.org/10.1016/j.cis.2011.11.001.
[21] M.C. Traub, W. Longsine, V.N. Truskett, Advances in nanoimprint lithography, Annu. Rev. Chem. Biomol. Eng. 7 (1) (2016) 583–604, https://doi.org/10.1146/annurev-chembioeng-080615-034635.
[22] E. Buitrago, T.S. Kulmala, R. Fallica, Y. Ekinci, EUV lithography process challenges, in: Frontiers of Nanoscience, vol. 11, Elsevier, 2016, pp. 135–176, https://doi.org/10.1016/B978-0-08-100354-1.00004-1.
[23] T.R. Groves, D. Pickard, B. Rafferty, N. Crosland, D. Adam, G. Schubert, Maskless electron beam lithography: prospects, progress, and challenges, Microelectron. Eng. 61–62 (2002) 285–293, https://doi.org/10.1016/S0167-9317(02)00528-2.
[24] Y. Chen, Nanofabrication by electron beam lithography and its applications: A review, Microelectron. Eng. 135 (2015) 57–72, https://doi.org/10.1016/j.mee.2015.02.042.
[25] W. Yao, H. Xu, H. Zhao, M. Tao, J. Liu, Fast and accurate proximity effect correction algorithm based on pattern edge shape adjustment for electron beam lithography, Microelectron. J. 133 (2023) 105718, https://doi.org/10.1016/j.mejo.2023.105718.
[26] M. Erdmanis, P. Sievilä, A. Shah, N. Chekurov, V. Ovchinnikov, I. Tittonen, Focused ion beam lithography for fabrication of suspended nanostructures on highly corrugated surfaces, Nanotechnology 25 (33) (2014) 335302, https://doi.org/10.1088/0957-4484/25/33/335302.
[27] V. Harinarayana, Y.C. Shin, Two-photon lithography for three-dimensional fabrication in micro/nanoscale regime: A comprehensive review, Optics Laser Technol. 142 (2021) 107180, https://doi.org/10.1016/j.optlastec.2021.107180.
[28] X. Zhou, Y. Hou, J. Lin, A review on the processing accuracy of two-photon polymerization, AIP Adv. 5 (3) (2015) 030701, https://doi.org/10.1063/1.4916886.
[29] S. Okazaki, High resolution optical lithography or high throughput electron beam lithography: The technical struggle from the micro to the nano-fabrication evolution, Microelectron. Eng. 133 (2015) 23–35, https://doi.org/10.1016/j.mee.2014.11.015.
[30] L.M. Cox, A.M. Martinez, A.K. Blevins, N. Sowan, Y. Ding, C.N. Bowman, Nanoimprint lithography: Emergent materials and methods of actuation, Nano Today 31 (2020) 100838, https://doi.org/10.1016/j.nantod.2019.100838.
[31] A.A. Tseng, Advancements and challenges in development of atomic force microscopy for nanofabrication, Nano Today 6 (5) (2011) 493–509, https://doi.org/10.1016/j.nantod.2011.08.003.
[32] R. Garcia, A.W. Knoll, E. Riedo, Advanced scanning probe lithography, Nature Nanotech 9 (8) (2014) 577–587, https://doi.org/10.1038/nnano.2014.157.
[33] P. Fan, et al., Scanning probe lithography: state-of-the-art and future perspectives, Micromachines 13 (2) (2022) 228, https://doi.org/10.3390/mi13020228.

[34] R. Garcia, Nanomechanical mapping of soft materials with the atomic force microscope: methods, theory and applications, Chem. Soc. Rev. 49 (16) (2020) 5850–5884, https://doi.org/10.1039/D0CS00318B.

[35] G. Binnig, C.F. Quate, Ch. Gerber, Atomic force microscope, Phys. Rev. Lett. 56 (9) (1986) 930–933, https://doi.org/10.1103/PhysRevLett.56.930.

[36] B. Voigtländer, *Scanning Probe Microscopy: Atomic Force Microscopy and Scanning Tunneling Microscopy*, 1st ed. 2015. in NanoScience and Technology. Berlin, Heidelberg: Springer Berlin Heidelberg : Imprint: Springer, 2015. doi: 10.1007/978-3-662-45240-0.

[37] G. Binnig, C. Gerber, E. Stoll, T.R. Albrecht, C.F. Quate, Atomic resolution with atomic force microscope, Europhys. Lett. 3 (12) (1987) 1281–1286, https://doi.org/10.1209/0295-5075/3/12/006.

[38] H. Hu, H. Kim, S. Somnath, Tip-based nanofabrication for scalable manufacturing, Micromachines 8 (3) (2017) 90, https://doi.org/10.3390/mi8030090.

[39] I.W. Rangelow, et al., Review article: active scanning probes: A versatile toolkit for fast imaging and emerging nanofabrication, J. Vacuum Sci. Technol. B, Nanotechnol. Microelectron. Mater. Proces. Measur. Phenomena 35 (6) (2017) 06G101, https://doi.org/10.1116/1.4992073.

[40] E.S. Snow, P.M. Campbell, Fabrication of Si nanostructures with an atomic force microscope, Appl. Phys. Lett. 64 (15) (1994) 1932–1934, https://doi.org/10.1063/1.111746.

[41] S.T. Howell, A. Grushina, F. Holzner, J. Brugger, Thermal scanning probe lithography—a review, Microsyst. Nanoeng. 6 (1) (2020) 21, https://doi.org/10.1038/s41378-019-0124-8.

[42] Y. Yang, W. Zhao, Fabrication of nanoscale to microscale 2.5D square patterns on metallic films by the coupling AFM lithography, J. Manuf. Proc. 46 (2019) 129–138, https://doi.org/10.1016/j.jmapro.2019.08.032.

[43] G. Liu, M. Hirtz, H. Fuchs, Z. Zheng, Development of Dip-Pen Nanolithography (DPN) and Its Derivatives, Small 15 (21) (2019) 1900564, https://doi.org/10.1002/smll.201900564.

[44] Y. Yan, S. Chang, T. Wang, and Y. Geng, "Scratch on Polymer Materials Using AFM Tip-Based Approach: A Review," p. 30, 2019.

[45] J. Gong, et al., Micro- and nanopatterning of inorganic and polymeric substrates by indentation lithography, Nano Lett. 10 (7) (2010) 2702–2708, https://doi.org/10.1021/nl101675s.

[46] Y. He, Y. Yan, Y. Geng, E. Brousseau, Fabrication of periodic nanostructures using dynamic plowing lithography with the tip of an atomic force microscope, Appl. Surf. Sci. 427 (2018) 1076–1083, https://doi.org/10.1016/j.apsusc.2017.08.134.

[47] S.V. Kontomaris, A. Malamou, Hertz model or Oliver & Pharr analysis? Tutorial regarding AFM nanoindentation experiments on biological samples, Mater. Res. Express 7 (3) (2020) 033001, https://doi.org/10.1088/2053-1591/ab79ce.

[48] S. Cárdenas-Pérez, J.J. Chanona-Pérez, J.V. Méndez-Méndez, I. Arzate-Vázquez, J.D. Hernández-Varela, N.G. Vera, Recent advances in atomic force microscopy for assessing the nanomechanical properties of food materials, Trends Food Sci. Technol. 87 (2019) 59–72, https://doi.org/10.1016/j.tifs.2018.04.011.

[49] N. Guz, M. Dokukin, V. Kalaparthi, I. Sokolov, If Cell Mechanics Can Be Described by Elastic Modulus: Study of Different Models and Probes Used in Indentation Experiments, Biophys. J . 107 (3) (2014) 564–575, https://doi.org/10.1016/j.bpj.2014.06.033.

[50] S.-V. Kontomaris, A. Stylianou, A. Malamou, T. Stylianopoulos, A discussion regarding the approximation of cylindrical and spherical shaped samples as half spaces in AFM nanoindentation experiments, Mater. Res. Express 5 (8) (2018) 085402, https://doi.org/10.1088/2053-1591/aad2c9.

[51] G.M. Pharr, W.C. Oliver, F.R. Brotzen, On the generality of the relationship among contact stiffness, contact area, and elastic modulus during indentation, J. Mater. Res. 7 (3) (1992) 613–617, https://doi.org/10.1557/JMR.1992.0613.

[52] N.M. Pugno, A general shape/size-effect law for nanoindentation, Acta Mater. 55 (6) (2007) 1947–1953, https://doi.org/10.1016/j.actamat.2006.10.053.

[53] L. Calabri, N. Pugno, C. Menozzi, and S. Valeri, "AFM nanoindentation: tip shape and tip radius of curvature effect on the hardness measurement," *J. Phys.: Condens. Matter*, vol. 20, no. 47, p. 474208, Nov. 2008, doi: 10.1088/0953-8984/20/47/474208.

[54] B. Du, O. K. C. Tsui, Q. Zhang, and T. He, "Study of Elastic Modulus and Yield Strength of Polymer Thin Films Using Atomic Force Microscopy," p. 6.

[55] M. Cascione, et al., Improvement of PMMA Dental Matrix Performance by Addition of Titanium Dioxide Nanoparticles and Clay Nanotubes, Nanomaterials 11 (8) (2021) 2027, https://doi.org/10.3390/nano11082027.

[56] K. Wiesauer, G. Springholz, Fabrication of semiconductor nanostructures by nanoindentation of photoresist layers using atomic force microscopy, J. Appl. Phys. 88 (12) (2000) 7289–7297, https://doi.org/10.1063/1.1324693.

[57] B. Cappella, H. Sturm, Comparison between dynamic plowing lithography and nanoindentation methods, J. Appl. Phys. 91 (1) (2002) 506, https://doi.org/10.1063/1.1421632.

[58] P. Pellegrino, et al., Pulse-atomic force lithography: a powerful nanofabrication technique to fabricate constant and varying-depth nanostructures, Nanomaterials 12 (6) (2022) 991, https://doi.org/10.3390/nano12060991.

[59] P. Pellegrino *et al.*, "Investigation of the Effects of Pulse-Atomic Force Nanolithography Parameters on 2.5D Nanostructures' Morphology," *Nanomaterials*, vol. 12, no. 24, p. 4421, Dec. 2022, doi: 10.3390/nano12244421.

[60] P. Pellegrino, et al., Pile-ups formation in AFM-Based nanolithography: morpho-mechanical characterization and removal strategies, Micromachines 13 (11) (2022) 1982, https://doi.org/10.3390/mi13111982.

[61] L.A. Porter, A.E. Ribbe, J.M. Buriak, Metallic nanostructures via static plowing lithography, Nano Lett. 3 (8) (2003) 1043–1047, https://doi.org/10.1021/nl034328c.

[62] A.A. Tseng, C.-F.-J. Kuo, S. Jou, S. Nishimura, J. Shirakashi, Scratch direction and threshold force in nanoscale scratching using atomic force microscopes, Appl. Surf. Sci. 257 (22) (2011) 9243–9250, https://doi.org/10.1016/j.apsusc.2011.04.065.

[63] A.A. Tseng, J. Shirakashi, S. Nishimura, K. Miyashita, A. Notargiacomo, Scratching properties of nickel-iron thin film and silicon using atomic force microscopy, J. Appl. Phys. 106 (4) (2009) 044314, https://doi.org/10.1063/1.3197313.

[64] A.A. Tseng, J. Shirakashi, S. Jou, J.-C. Huang, T.P. Chen, Scratch properties of nickel thin films using atomic force microscopy, J. Vac. Sci. Technol., B: Nanotechnol. Microelectron.: Mater., Process., Meas., Phenom. 28 (1) (2010) 202–210, https://doi.org/10.1116/1.3292944.

[65] A.A. Tseng, J.-I. Shirakashi, S. Nishimura, K. Miyashita, Z. Li, Nanomachining of Permalloy for Fabricating Nanoscale Ferromagnetic Structures Using Atomic Force Microscopy, J. Nanosci. Nanotech. 10 (1) (2010) 456–466, https://doi.org/10.1166/jnn.2010.1797.

[66] R. Suda, T. Ohyama, A. A. Tseng, and J. Shirakashi, "In-situ control of quantum point contacts using scanning probe microscopy scratch lithography," in *2012 12th IEEE International Conference on Nanotechnology (IEEE-NANO)*, Birmingham, United Kingdom: IEEE, Aug. 2012, pp. 1–5. doi: 10.1109/NANO.2012.6321908.

[67] S.B. Ulapane, J.L. Doolin, M.K. Okeowo, C.L. Berrie, Atomic force microscopy-based static plowing lithography Using $CaCO_3$ nanoparticle resist layers as a substrate-flexible selective metal deposition resist, J. Phys. Chem. C 125 (42) (2021) 23490–23500, https://doi.org/10.1021/acs.jpcc.1c07239.

[68] C.M. Edwards, S.B. Ulapane, N.J.B. Kamathewatta, H.M. Ashberry, C.L. Berrie, Fabrication and growth control of metal nanostructures through exploration of atomic force microscopy-based patterning and electroless deposition conditions, J. Phys. Chem. C 124 (46) (2020) 25588–25601, https://doi.org/10.1021/acs.jpcc.0c08017.

[69] G.-Y. Liu, S. Xu, Y. Qian, Nanofabrication of self-assembled monolayers using scanning probe lithography, Acc. Chem. Res. 33 (7) (2000) 457–466, https://doi.org/10.1021/ar980081s.

[70] Y. Geng, B. Yu, Y. Yan, Z. Hu, X. Zhao, Direction-identical scratching method for fabricating nanostructures using a modified AFM nanoscratching system, J. Vac. Sci. Technol., B: Nanotechnol. Microelectron.: Mater., Process., Meas., Phenom. 33 (2) (2015) 021802, https://doi.org/10.1116/1.4906790.

[71] Y. Yan, Y. Sun, J. Li, Z. Hu, X. Zhao, Controlled nanodot fabrication by rippling polycarbonate surface using an AFM diamond tip, Nanoscale Res Lett 9 (1) (2014) 372, https://doi.org/10.1186/1556-276X-9-372.

[72] G. Xiao, Y. He, Y. Geng, Y. Yan, M. Ren, Molecular dynamics and experimental study on comparison between static and dynamic ploughing lithography of single crystal copper, Appl. Surf. Sci. 463 (2019) 96–104, https://doi.org/10.1016/j.apsusc.2018.08.204.

[73] Y. He, Y. Yan, Y. Geng, Z. Hu, Fabrication of none-ridge nanogrooves with large-radius probe on PMMA thin-film using AFM tip-based dynamic plowing lithography approach, J. Manuf. Process. 29 (2017) 204–210, https://doi.org/10.1016/j.jmapro.2017.07.016.

[74] B. Vasić, et al., Atomic force microscopy based manipulation of graphene using dynamic plowing lithography, Nanotechnology 24 (1) (2013) 015303, https://doi.org/10.1088/0957-4484/24/1/015303.

[75] M. Heyde, et al., Dynamic plowing nanolithography on polymethylmethacrylate using an atomic force microscope, Rev. Sci. Instrum. 72 (1) (2001) 136–141, https://doi.org/10.1063/1.1326053.

[76] B. Cappella, H. Sturm, S.M. Weidner, Breaking polymer chains by dynamic plowing lithography, Polymer 43 (16) (2002) 4461–4466, https://doi.org/10.1016/S0032-3861(02)00285-9.

[77] Y. Yan, Y. He, Y. Geng, Z. Hu, X. Zhao, Characterization study on machining PMMA thin-film using AFM tip-based dynamic plowing lithography: Characterization study on machining PMMA thin-film, Scanning 38 (6) (2016) 612–618, https://doi.org/10.1002/sca.21308.

[78] I. Stoica, A.I. Barzic, C. Hulubei, Fabrication of nanochannels on polyimide films using dynamic plowing lithography, Appl. Surf. Sci. 426 (2017) 307–314, https://doi.org/10.1016/j.apsusc.2017.07.214.

[79] A.G. Jones, C. Balocco, R. King, A.M. Song, Highly tunable, high-throughput nanolithography based on strained regioregular conducting polymer films, Appl. Phys. Lett. 89 (1) (2006) 013119, https://doi.org/10.1063/1.2219094.

[80] Y. He, Y. Geng, Y. Yan, X. Luo, Fabrication of Nanoscale Pits with High Throughput on Polymer Thin Film Using AFM Tip-Based Dynamic Plowing Lithography, Nanoscale Res Lett 12 (1) (2017) 544, https://doi.org/10.1186/s11671-017-2319-y.

[81] Y. He, Y. Yan, J. Wang, Y. Geng, B. Xue, X. Zhao, Study on the Effects of the Machining Parameters on the Fabrication of Nanoscale Pits Using the Dynamic Plowing Lithography Approach, IEEE Trans. Nanotechnology 18 (2019) 351–357, https://doi.org/10.1109/TNANO.2019.2904336.

[82] L. Zhang, J. Dong, High-rate tunable ultrasonic force regulated nanomachining lithography with an atomic force microscope, Nanotechnology 23 (8) (2012) 085303, https://doi.org/10.1088/0957-4484/23/8/085303.

[83] J. Deng, J. Dong, P. Cohen, High Rate 3D nanofabrication by AFM-based ultrasonic vibration assisted nanomachining, Procedia Manuf. 5 (2016) 1283–1294, https://doi.org/10.1016/j.promfg.2016.08.100.

[84] J. Deng, L. Jiang, B. Si, H. Zhou, J. Dong, P. Cohen, AFM-Based nanofabrication and quality inspection of three-dimensional nanotemplates for soft lithography, J. Manuf. Process. 66 (2021) 565–573, https://doi.org/10.1016/j.jmapro.2021.04.051.

[85] L. Zhang, J. Dong, P.H. Cohen, Material-insensitive feature depth control and machining force reduction by ultrasonic vibration in AFM-based nanomachining,

IEEE Trans. Nanotechnology 12 (5) (2013) 743–750, https://doi.org/10.1109/TNANO.2013.2273272.
[86] J. Shi, L. Liu, P. Zhou, F. Wang, Y. Wang, Subnanomachining by ultrasonic-vibration-assisted atomic force microscopy, IEEE Trans. Nanotechnology 14 (4) (2015) 735–741, https://doi.org/10.1109/TNANO.2015.2439311.
[87] J. Melcher, S. Hu, A. Raman, Equivalent point-mass models of continuous atomic force microscope probes, Appl. Phys. Lett. 91 (5) (2007) 053101, https://doi.org/10.1063/1.2767173.
[88] O. K. Oleg Kolosov and K. Y. Kazushi Yamanaka, "Nonlinear Detection of Ultrasonic Vibrations in an Atomic Force Microscope," *Jpn. J. Appl. Phys.*, vol. 32, no. 8A, p. L1095, Aug. 1993, doi: 10.1143/JJAP.32.L1095.
[89] J. Shi, L. Liu, G. Li, The co-design of interface sensing and tailoring of ultra-thin film with ultrasonic vibration-assisted AFM system, Nanotechnology 27 (23) (2016) 235302, https://doi.org/10.1088/0957-4484/27/23/235302.
[90] J. Shi, L. Liu, P. Yu, Y. Cong, G. Li, Phase shifting-based debris effect detection in USV-assisted AFM nanomachining, Appl. Surf. Sci. 413 (2017) 317–326, https://doi.org/10.1016/j.apsusc.2017.03.218.
[91] J. Deng, L. Zhang, J. Dong, P.H. Cohen, AFM-based 3D nanofabrication using ultrasonic vibration assisted nanomachining, Procedia Manuf. 1 (2015) 584–592, https://doi.org/10.1016/j.promfg.2015.09.036.
[92] J. Deng, L. Zhang, J. Dong, P.H. Cohen, AFM-based 3D nanofabrication using ultrasonic vibration assisted nanomachining, J. Manuf. Process. 24 (2016) 195–202, https://doi.org/10.1016/j.jmapro.2016.09.003.
[93] J. Deng, J. Dong, P.H. Cohen, Development and characterization of ultrasonic vibration assisted nanomachining process for three-dimensional nanofabrication, IEEE Trans. Nanotechnol. 17 (3) (2018) 559–566, https://doi.org/10.1109/TNANO.2018.2826841.
[94] J. Deng, H. Zhou, J. Dong, P. Cohen, Three-dimensional nanomolds fabrication for nanoimprint lithography, Procedia Manuf. 34 (2019) 228–232, https://doi.org/10.1016/j.promfg.2019.06.143.
[95] H. Zhou, J. Deng, Vibration assisted AFM-based nanomachining under elevated temperatures using soft and stiff probes, Procedia Manuf. 48 (2020) 508–513, https://doi.org/10.1016/j.promfg.2020.05.075.
[96] B.A. Gozen, O.B. Ozdoganlar, A rotating-tip-based mechanical nano-manufacturing process: nanomilling, Nanoscale Res Lett 5 (9) (2010) 1403–1407, https://doi.org/10.1007/s11671-010-9653-7.
[97] B.A. Gozen, O.B. Ozdoganlar, Design and evaluation of a mechanical nanomanufacturing system for nanomilling, Precis. Eng. 36 (1) (2012) 19–30, https://doi.org/10.1016/j.precisioneng.2011.06.001.
[98] B. Arda Gozen and O. Burak Ozdoganlar, "Wear of ultrananocrystalline diamond AFM tips during mechanical nanomanufacturing by nanomilling," *Wear*, vol. 317, no. 1–2, pp. 39–55, Sep. 2014, doi: 10.1016/j.wear.2014.04.024.
[99] Y. Geng, Y. Yan, Y. Xing, X. Zhao, Z. Hu, Modelling and experimental study of machined depth in AFM-based milling of nanochannels, Int J Mach Tool Manu 73 (2013) 87–96, https://doi.org/10.1016/j.ijmachtools.2013.07.001.
[100] Y. Geng, H. Li, Y. Yan, Y. He, X. Zhao, Study on material removal for nanochannels fabrication using atomic force microscopy tip-based nanomilling approach, Proc. Inst. Mech. Eng. B J. Eng. Manuf. 233 (2) (2019) 461–469, https://doi.org/10.1177/0954405417748188.
[101] Y. Geng, J. Wang, H. Li, Y. Yan, Study on the effects of feed directions on chip formation and machined depth when implementing nanoscratching by nanomilling approach, Procedia CIRP 71 (2018) 285–288, https://doi.org/10.1016/j.procir.2018.05.014.
[102] D. Cui, L. Zhang, K. Mylvaganam, W. Liu, W. Xu, Nano-milling on monocrystalline copper: A molecular dynamics simulation, Mach. Sci. Technol. 21 (1) (2017) 67–85, https://doi.org/10.1080/10910344.2016.1260430.
[103] Y. Yan, Z. Li, J. Wang, Y. Geng, Atomic simulations of tip-based nanomilling on single-crystal copper, Mater. Today Commun. 31 (2022) 103709, https://doi.org/10.1016/j.mtcomm.2022.103709.
[104] J. Wang, Y. Yan, Z. Li, Y. Geng, X. Luo, P. Fan, Processing outcomes of atomic force microscope tip-based nanomilling with different trajectories on single-crystal silicon, Precis. Eng. 72 (2021) 480–490, https://doi.org/10.1016/j.precisioneng.2021.06.009.
[105] Y. Yan, J. Wang, Y. Geng, G. Zhang, Material removal mechanism of multi-layer metal-film nanomilling, CIRP Ann. 71 (1) (2022) 61–64, https://doi.org/10.1016/j.cirp.2022.03.040.
[106] J. Wang, Y. Yan, Z. Li, Y. Geng, Towards understanding the machining mechanism of the atomic force microscopy tip-based nanomilling process, Int J Mach Tool Manu 162 (2021) 103701, https://doi.org/10.1016/j.ijmachtools.2021.103701.
[107] H.J. Mamin, D. Rugar, Thermomechanical writing with an atomic force microscope tip, Appl. Phys. Lett. 61 (8) (1992) 1003–1005, https://doi.org/10.1063/1.108460.
[108] H.F. Hamann, M. O'Boyle, Y.C. Martin, M. Rooks, H.K. Wickramasinghe, Ultra-high-density phase-change storage and memory, Nature Mater 5 (5) (2006) 383–387, https://doi.org/10.1038/nmat1627.
[109] W.P. King, et al., Heated atomic force microscope cantilevers and their applications, Ann. Rev Heat Transfer 16 (1) (2013) 287–326, https://doi.org/10.1615/AnnualRevHeatTransfer.v16.100.
[110] W.P. King, S. Saxena, B.A. Nelson, B.L. Weeks, R. Pitchimani, Nanoscale thermal analysis of an energetic material, Nano Lett. 6 (9) (2006) 2145–2149, https://doi.org/10.1021/nl061196p.
[111] D. Pires, et al., Nanoscale three-dimensional patterning of molecular resists by scanning probes, Science 328 (5979) (2010) 732–735, https://doi.org/10.1126/science.1187851.
[112] P.C. Paul, A.W. Knoll, F. Holzner, M. Despont, U. Duerig, Rapid turnaround scanning probe nanolithography, Nanotechnology 22 (27) (2011) 275306, https://doi.org/10.1088/0957-4484/22/27/275306.
[113] C.D. Rawlings, et al., Control of the interaction strength of photonic molecules by nanometer precise 3D fabrication, Sci Rep 7 (1) (2017) 16502, https://doi.org/10.1038/s41598-017-16496-x.
[114] S. Saxena, Nanoscale thermal lithography by local polymer decomposition using a heated atomic force microscope cantilever tip, J. Micro/Nanolith. MEMS MOEMS 6 (2) (2007) 023012, https://doi.org/10.1117/1.2743374.
[115] Y. Hua, W.P. King, C.L. Henderson, Nanopatterning materials using area selective atomic layer deposition in conjunction with thermochemical surface modification via heated AFM cantilever probe lithography, Microelectron. Eng. 85 (5–6) (2008) 934–936, https://doi.org/10.1016/j.mee.2008.01.105.
[116] C. Neuber, Molecular glass resists for scanning probe lithography, in: D. J. Resnick, C. Bencher (Eds.), Presented at the SPIE Advanced Lithography, San Jose, California, United States, 2014, p. 90491V, 10.1117/12.2047108.
[117] A. De Silva, et al., Study of the structure−properties relationship of phenolic molecular glass resists for next generation photolithography, Chem. Mater. 20 (4) (2008) 1606–1613, https://doi.org/10.1021/cm702613n.
[118] O. Coulembier, et al., Probe-based nanolithography: self-amplified depolymerization media for dry lithography, Macromolecules 43 (1) (2010) 572–574, https://doi.org/10.1021/ma9019152.
[119] F. Holzner, et al., Directed placement of gold nanorods using a removable template for guided assembly, Nano Lett. 11 (9) (2011) 3957–3962, https://doi.org/10.1021/nl202276q.
[120] S. Chang, Y. Yan, B. Li, Y. Geng, Nanoscale manipulation of materials patterning through thermomechanical nanolithography using atomic force microscopy, Mater. Des. 202 (2021) 109547, https://doi.org/10.1016/j.matdes.2021.109547.
[121] Y.K. Ryu Cho, et al., Sub-10 nanometer feature size in silicon using thermal scanning probe lithography, ACS Nano 11 (12) (2017) 11890–11897, https://doi.org/10.1021/acsnano.7b06307.
[122] P. Vettiger, et al., The 'Millipede'—More than thousand tips for future AFM storage, IBM J. Res. & Dev. 44 (3) (2000) 323–340, https://doi.org/10.1147/rd.443.0323.
[123] N. Lassaline, et al., Optical fourier surfaces, Nature 582 (7813) (2020) 506–510, https://doi.org/10.1038/s41586-020-2390-x.
[124] X. Zheng, et al., Patterning metal contacts on monolayer MoS2 with vanishing Schottky barriers using thermal nanolithography, Nat Electron 2 (1) (2019) 17–25, https://doi.org/10.1038/s41928-018-0191-0.
[125] Z. Li, et al., Achieving reliable and ultrafast memristors via artificial filaments in silk fibroin, Adv. Mater. 36 (4) (2024) 2308843, https://doi.org/10.1002/adma.202308843.
[126] S. Sadewasser, C. Barth, Electrostatic force microscopy and kelvin probe force microscopy, in: E.N. Kaufmann (Ed.), Characterization of Materials, John Wiley & Sons Inc, Hoboken, NJ, USA, 2012, p. p. com152., https://doi.org/10.1002/0471266965.com152.
[127] Y.-R. Ma, C. Yu, Y.-D. Yao, Y. Liou, S.-F. Lee, Tip-induced local anodic oxidation on the native SiO 2 layer of Si(111) using an atomic force microscope, Phys. Rev. B 64 (19) (2001) 195324, https://doi.org/10.1103/PhysRevB.64.195324.
[128] B. Legrand, D. Deresmes, D. Stiévenard, Silicon nanowires with sub 10 nm lateral dimensions: From atomic force microscope lithography based fabrication to electrical measurements, J. Vac. Sci. Technol. B 20 (3) (2002) 862, https://doi.org/10.1116/1.1470519.
[129] S. Myhra, Tip-induced local anodic oxidation: nanolithography and nanobiotechnology, Nanobiotechnol 3 (3–4) (2007) 212–222, https://doi.org/10.1007/s12030-008-9014-0.
[130] L. A. Cohen et al., "Tunable fractional quantum Hall point contacts in graphene via local anodic oxidation of graphite gates." arXiv, Apr. 22, 2022. Accessed: Mar. 28, 2023. [Online]. Available: http://arxiv.org/abs/2204.10296.
[131] G. Lee, et al., Experimental and numerical study of electrochemical nanomachining using an AFM cantilever tip, Nanotechnology 21 (18) (2010) 185301, https://doi.org/10.1088/0957-4484/21/18/185301.